Elucidation of Battery Electrolyte Coordination Sphere Thermodynamics via Calorimetric and Potentiometric Titrations

by

Dhyllan A. Skiba

B.S. in Mechanical Engineering
B.S. in Computer Engineering
Boston University, 2021

Submitted to the Department of Mechanical Engineering
in Partial Fulfilment of the Requirements of the Degree of

MASTER OF SCIENCE IN MECHANICAL ENGINEERING

at the

MASSACHUSETTS INSTITUTE OF TECHNOLOGY

February 2024

Authored by: Dhyllan A. Skiba
Department of Mechanical Engineering
January 19, 2024

Certified by: Betar M. Gallant
Professor of Mechanical Engineering, Thesis Supervisor

Accepted by: Nicolas Hadjiconstantinou
Chairman, Department Committee on Graduate Theses

Elucidation of Battery Electrolyte Coordination Sphere Thermodynamics via Calorimetric and Potentiometric Titrations

by

Dhyllan A. Skiba

Submitted to the
Department of Mechanical Engineering
on January 19. 2024 in Partial Fulfilment of the
Requirements of the Degree of
Master of Science in Mechanical Engineering

ABSTRACT

Rechargeable metal-anode batteries are a promising post Li-ion battery development. However, the high reactivity of metallic anodes with the electrolyte results in the formation of a solid-electrolyte interphase (SEI). Electrolyte design is a key handle in controlling the SEI composition in metal-anode batteries, but our understanding of the electrolyte—specifically the cation's first coordination sphere—is limited. In this thesis, the study of ion solvation and complexation techniques are brought into the context of battery electrolytes. Relevant data from literature is summarized and supplemented with enthalpy of solution ($\Delta_{\mathrm{sol}}\mathrm{H}$) and enthalpy of transfer ($\Delta_{\mathrm{tr}}\mathrm{H}$) measurements for the Li-battery relevant salts, $LiPF_6$ and LiTFSI, in a set of polar aprotic solvents. The trends observed are rationalized by consideration of solvent and anion properties, particularly the solvent donicity and anion size. To achieve a finer picture of the Li^+ coordination sphere, isothermal titration calorimetry (ITC) and potentiometric titrations (PT) were employed with a set of exemplar electrolytes to probe the thermodynamic evolution of the Li^+ coordination complex as weak solvent is displaced by a stronger solvent in the first coordination sphere. Raman spectroscopy is used to confirm that solvent displacement occurs as expected, and the effect of the anion on ITC measurements is investigated. A statistical binding model is developed which is fit to the experimental titration data to extract an average change in Gibbs free energy ($\Delta\mathrm{G}$), enthalpy ($\Delta\mathrm{H}$), and entropy ($\Delta\mathrm{S}$) of solvent displacement. Preferential solvation tendencies are quantified for EC:DMC and EC:PC electrolyte using this methodology, and compared with preferences observed by other workers. This thesis provides the framework for future studies on the thermodynamics of more complex battery electrolyte coordination environments and its connection with the SEI composition.

Thesis Supervisor: Betar M. Gallant

Title: Associate Professor of Mechanical Engineering

Acknowledgements

I would first like to thank my advisor, Professor Betar M. Gallant, for her phenomenal guidance and support throughout my master's degree, and for her kindness, patience, and curiosity which have inspired me throughout my research and in life. I would also like to thank my colleagues Dr. Maryam Abdinejad, Dr. Haining Gao, Dr. Rui Guo, Dr. Gustavo Hobold, Dr. Sung Eun Jerng, Dr. Kyeong-Ho Kim, Dr. Graham Leverick, Elizabeth Bernhardt, Gi-Hyun Byun, Kyle Jiang, Lorenz Kopp, Fang-Yu Kuo, Dharmjeet Madhav, Aaron Melemed, Stephanie Ross, Benedikt Schultes, Alejandro Sevilla, Katherine Steinberg, and Zheng Yong Toh for the many interesting discussions, and for their friendship which has made my time at MIT such a great experience. I am also incredibly grateful for the encouragement from my friends and family, and I am especially grateful to my parents and my twin sister, Izabelle, for their unwavering love and support.

I gratefully acknowledge financial support during my master's degree from a National Science Foundation CAREER award; from the MIT Department of Mechanical Engineering Prof. Warren M. Rohsenow Fellowship; and from a MathWorks Fellowship. This work made use of the MIT Materials Research Science and Engineering Center Shared Experimental Facilities (MRSEC), supported by the National Science Foundation under award number DMR-14-19807.

Contents

List of Figures

List of Tables

Solvent Properties

Solvent Acronym	Solvent Name	DN (kcal/mol)	ε
ACN	acetonitrile	14.1	37.5
DEC	diethyl carbonate	16.0	2.82
Diglyme	bis(2-methoxyethyl) ether	19	7.3
DMA	N,N-dimethylacetamide	27.8	37.8
DMC	dimethyl carbonate	17.2	3.1
DME (monoglyme)	1,2-dimethoxyethane	23.9	7.2
DMF	N,N-dimethylformamide	26.6	36.7
DMSO	dimethyl sulfoxide	29.8	46.7
DOL	1,3-dioxolane	21.2	7.34
EC	ethylene carbonate	16.4	89.6
HMPA	hexamethylphosphoramide	38.8	30
MeIm	1-methylimidazole	47.0	40
MeTHF	2-methyltetrahydrofuran	12	6.97
NMP	N-methyl-2-pyrrolidone	27.3	33
PC	propylene carbonate	15.1	66.1
SL (sulfolane)	tetramethylene sulfone	14.8	43.3
THF	tetrahydrofuran	20	7.58
triglyme	triethylene glycol dimethyl ether	14	7.5

I. Introduction & Background

One of the key checkpoints in reaching net zero carbon emissions is vehicle electrification.[4] As such, there has been an increasing demand for more energy dense, faster-charging, safer, and cheaper batteries which can enable mass adoption of electric vehicles (EVs). The current state of the art are Li-ion batteries (LIBs) which offer specific energies up to 260 Wh/kg. However, LIBs are reaching maturity and are not yet energy dense enough or cheap enough to meet DOE goals (>350 Wh/kg and <$100/Wh) to be competitive with combustion engine vehicles.[5, 6] Further, although the price of LIBs have been declining, they still have fire safety concerns and have limited charging speeds due to intercalation kinetics within the anode and cathode. As such, it has become imperative that battery chemistries beyond Li-ion are developed.

I.1. Metallic Anodes and the Solid Electrolyte Interphase

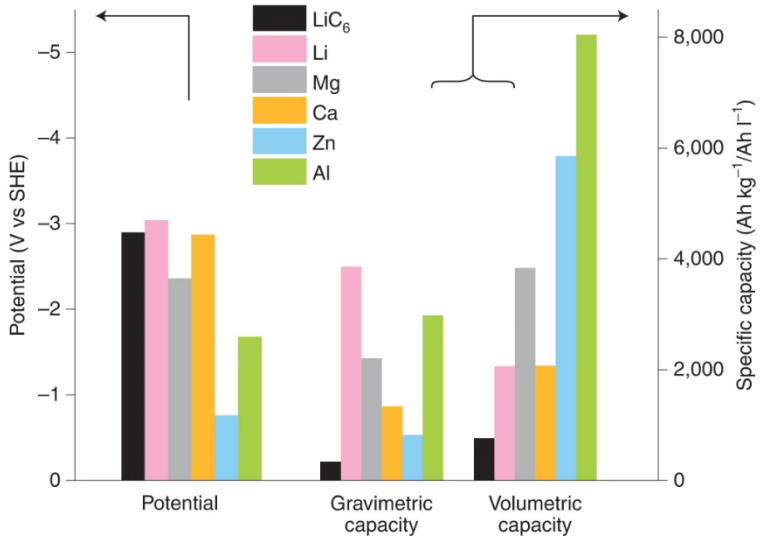

Figure I.1: ***Comparison of metallic anodes vs. a graphitic Li-ion intercalation anode.*** *Potential, theoretical gravimetric capacity, and theoretical volumetric capacity of LiC_6, Li, Mg, Ca, Zn, and Al anodes. Figure reproduced from Y. Liang et al.* Nature Energy ***2020***.[1]

Metallic anodes are a promising advancement upon the graphitic intercalation anodes found in state-of-the-art LIBs. As seen in Figure I.1, using a metallic anode can offer significant increases in gravimetric and volumetric capacities, which in turn improves specific energy and may improve charging speeds by removing the intercalation bottleneck. A Li anode is the ideal choice given its highest theoretical gravimetric capacity and lowest electrochemical potential compared to all other known anode materials (3,860 mAh/g and -3.04 V vs. SHE respectively).[7, 8] Using metallic Li as the anode is proposed to offer up to 50% increases in battery specific energy from ~260 Wh/kg (graphitic anode), to ~440 Wh/kg (Li anode).[9] Further specific energy improvements can be made by replacing the transition-metal-oxide intercalation cathode found in Li-ion batteries with a non-intercalating cathode such as a sulfur or oxygen cathode, each of which suffers from their own challenges, not covered here. Other possible metallic anode choices include Na, K, Ca, Zn, Mg, and Al.[1, 10-12] Li anodes are by far the most investigated and considerable progress has been made to bring Li metal batteries to the commercial market; nevertheless, there are still several challenges including dendrite formation/safety issues, high cost, and limited Li supply. Any of the alternative metallic anodes listed above are substantially more abundant than Li and may alleviate supply and cost issues. Additionally, Mg and Ca exhibit resistance to dendritic growth at moderate charging current densities offering possible safety benefits.[1] Ca-based batteries are particularly interesting as a long term sustainable alternative to Li due to the approximately 2000x higher abundance of Ca in the Earth's crust, a low electrochemical redox potential of -2.97 V vs. SHE which is closer to Li (-3.04 V vs. SHE) than other metal anode alternatives, and a theoretical volumetric capacity of 2073 mAh/cc comparable to Li (2062 mAh/cc).[13, 14]

The primary challenge for all metallic anodes, however, is their reactivity with the liquid electrolyte. Electrolyte components either chemically or electrochemically react at the surface of the metal due to

thermodynamic instability at the low redox potential of the anode.[15] The solid decomposition products form what is known as the solid-electrolyte interphase (SEI). The SEI needs to fully passivate the anode surface, be electrically insulating, ionically conductive, and stable over continuous cycling to enable long-term battery life. Over the past few decades, Li metal battery development has seen two major approaches to improving battery efficiencies: interfacial engineering (such as artificial SEI's), and electrolyte engineering.[7, 16, 17] Electrolyte engineering has proven to be a powerful approach to achieve >99% coulombic efficiencies in Li metal batteries.[18, 19] Researchers have found that the molecules in the primary cation coordination sphere—the nearest molecules that are electrostatically coordinated to the cation in the electrolyte—are a dominant source of decomposition products.[3, 19-27] For example, S.C. Kim et al. measured relative differences in Gibbs free energy of solvation of Li^+ using a symmetric-electrode asymmetric-electrolyte H-cell setup and showed that when using a more strongly Li-binding solvent (DME), the SEI composition is dominated by solvent-derived organic products, whereas when using a more weakly Li-binding solvent (FDMB), the SEI composition is dominated by anion-derived inorganic products.[20] The trend holds for other metal anodes too. For example, Hou et al. constructed a Ca|Ca symmetric cell with a $Ca(TFSI)_2$ electrolyte in 3 different solvents: EC:PC, DMA, and MeIm. They found that when using the weakly Ca-binding EC:PC solvent, there was significant ion pairing that resulted in increased anion-derived CaF_2 content in the SEI, and when using the strongly Ca-binding solvents DMA and MeIm, ion pairing, along with CaF_2 in the SEI, was minimized.[25]

This behavior is reasoned by considering the transport of ions in solution. When cations are driven to the surface of the anode during charging, they also bring their coordination sphere directly to the anode surface, which facilitates decomposition of these molecules. Additionally, ion coordination tends to lower the LUMO energy of the coordinated molecules, making reduction from the coordination sphere easier than reduction of bulk molecules.[22] Using this idea, the Li-metal battery community have put

much effort into promoting the coordination of fluorinated anions with Li^+, which has allowed for the formation of more beneficial anion-derived phases in the SEI. While promoting ion pairing has worked well with Li, the same trend doesn't necessarily transfer to other metal anodes. In Ca, for example, only a handful of electrolytes have been found that form a functional SEI, with a major design motif of minimizing ion-pairing.[13, 28] New electrolyte design principles must be developed to form beneficial SEI's on other metal anodes. In order to better understand how the electrolyte impacts the formation and composition of the SEI, it has become necessary for researchers to develop methods for investigating the coordination environment around the cation.

I.2. The Electrolyte Coordination Sphere and Ion-Pairing

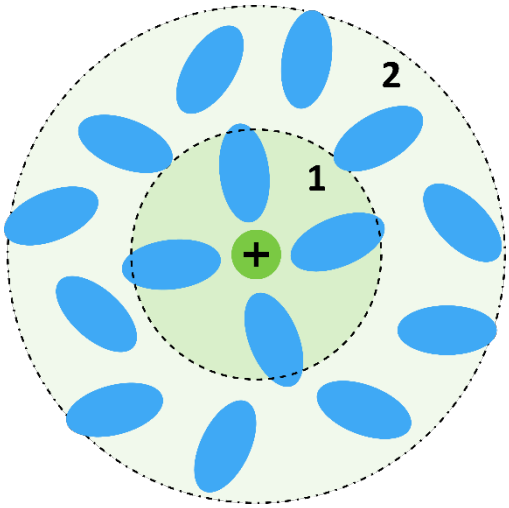

Figure I.2: ***Coordination spheres of a cation.*** *The green circle represents a cation, and the blue ovals represent other molecules which can coordinate to the central ion (i.e. solvent or anions). The inner dashed circle defines the first coordination sphere, and the outer defines the second coordination sphere.*

The environment around an ion in solution is typically referred to as the coordination sphere or the solvation shell. The term "coordination sphere" applies more generally to all complexation of an ion with other ions, solvents, and other neutral molecules in solution, whereas "solvation shell" is used to refer to the solvent structure around any solute, ionic or not. In the context of this work, the use of the term "coordination sphere" is more accurate because the environment around ions in battery electrolytes is typically comprised of more than just solvent.

More specifically, the first, or primary, cation coordination sphere refers to the ligands which are directly bound to the central cation. These ligands, also known as complexing agents in the field of complexation chemistry, are Lewis bases and can be neutral species or anions. They typically form co-ordinate, or dative covalent, bonds with the central ion, in which a lone pair of electrons from the ligand is shared with the ion, but there are exceptions for more specific chemical interactions. Outside of the first coordination sphere, there is a layer of solvents/ligands which don't directly form a bond with the

central cation, but also don't behave quite like bulk molecules. This layer is referred to as the second(ary) coordination shell. In aqueous solutions, this layer is typically characterized by hydrogen bonding of water with the ligands in the first coordination sphere. In non-aqueous aprotic solutions, there is comparatively less ordering in the second coordination sphere, but long-range ion-dipole and van der Waals forces still distinguish these molecules from the bulk. In all solutions however, the molecules in the second coordination sphere have weaker interaction with the central ion than molecules in the first coordination sphere. And thus, the residence times of molecules in the second coordination sphere tend to be shorter than the those in the first; the magnitude of this difference is strongly dependent on the specific ion and ligands. [29, 30]

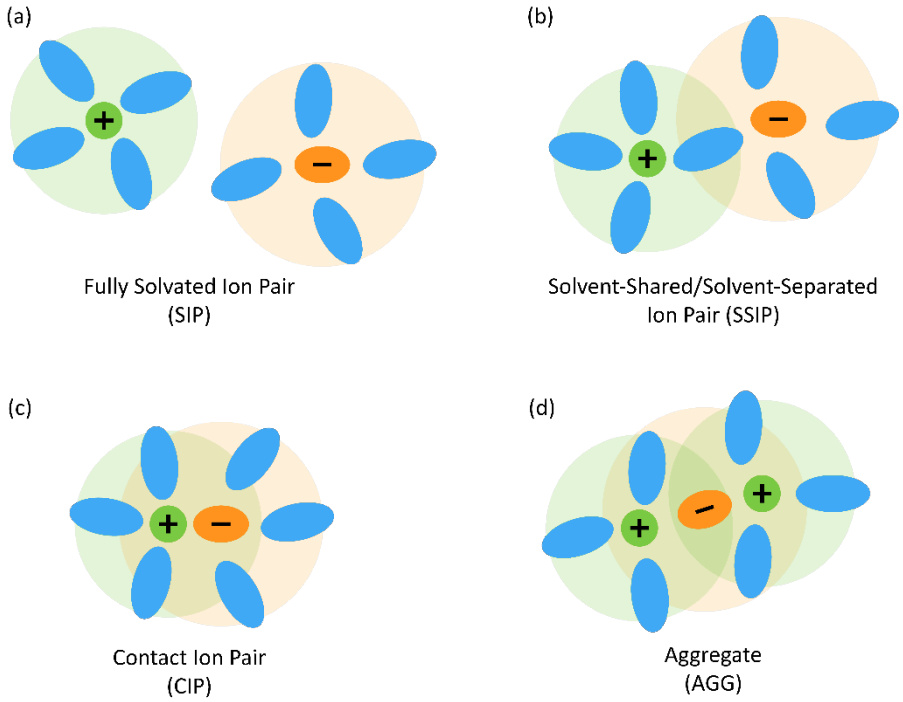

Figure I.3: ***Types of ion pairing in solution.*** *Solid green circles represent cations, and the larger concentric green circles represent the first coordination sphere of the cation. Similarly, solid orange ovals represent anions, and the larger concentric orange circles represent the first coordination sphere of the anion. Blue ovals represent solvents.*

As mentioned above, the first or second coordination sphere of a cation can, and commonly does, include an anion (possibly more than one). In any solution with cations, it is required that there are also anions for charge neutrality. The ions will naturally always form pairs due to the electrostatic forces between them, but the degree/strength of ion pairing varies based on the ion and solvent properties. In the context of the cation coordination sphere layers discussed, there are four types of ion pairing: fully solvated ion pair (SIP), solvent-separated/solvent-shared ion pair (SSIP), contact ion pair (CIP), and aggregates (AGG).

Fully solvated ion pairs, SIPs, are defined when the anion is outside the first and second cation coordination spheres, such that there are two or more solvent molecules that separate the cation and anion (Figure I.3a). In this case, the ion-ion interactions are much weaker than the solvent-ion coordination strengths. For moderately stronger ion-ion forces, solvent separated/shared ion pairs are formed. SSIPs are characterized by an anion in the second coordination sphere of the cation, where the anion and cation are separated by a single solvent molecule (Figure I.3b). Generally, it is challenging to distinguish between SSIPs and SIPs with experimental techniques and they are usually distinguished with molecular simulation.

CIPs are characterized by an anion in the first coordination sphere of the cation (Figure I.3c). This typically occurs because the solvent/ligand coordination isn't strong enough to separate the ions, or simply because there aren't enough solvents/ligands to fully coordinate every cation in solution. Another important consideration is the charge-shielding ability of the first coordination sphere, which is strongly dependent on the relative permittivity (or dielectric constant) of the solvents/ligands. High relative permittivity in the first coordination sphere greatly reduces the electrostatic interaction strength between the ions and supports the dissociation of CIPs into SSIPs or SIPs. Lastly, it is also possible for ions to form aggregates (AGG) in which two or more cations share anions, as CIPs, in their

first coordination shells (Figure I.3d). Aggregation is usually associated with distinct changes in macroscopic electrolyte properties such as viscosity and ionic conductivity.

I.3. Current Approaches in Probing Electrolyte Cation Coordination

As mentioned previously, researchers in the field of lithium metal batteries (LMBs) have made remarkable strides in tailoring the electrolyte coordination sphere to achieve desired properties in both the electrolyte and SEI. By strategically selecting solvents and fine-tuning their composition, researchers have been able to achieve semi-controlled ion coordination and, consequently, influence critical electrolyte and SEI properties. This deliberate design approach has allowed for the optimization of key electrolyte properties such as viscosity, conductivity, and compatibility with Li metal anodes. Moreover, researchers have been able to tailor the Li^+ coordination sphere to promote SEI phases that are perceived as beneficial to the SEI such as LiF.[18, 20, 31, 32] This targeted control of electrolyte solvation environments has been enabled by a variety of spectroscopic and computational methods which can quantitatively probe the bulk electrolyte cation coordination sphere composition and qualitatively rank Li^+ solvation strength.

I.3.1. Spectroscopic Approaches

The most common spectroscopic techniques used for studying the cation coordination sphere are Raman, Fourier transform infrared (FTIR), and nuclear magnetic resonance (NMR). Other techniques including electrospray ionization mass spectroscopy (ESI-MS) and dielectric relaxation spectroscopy (DRS) have been used as well. Raman and FTIR are both nondestructive spectroscopic techniques which are sensitive to changes in the vibrational modes of the molecules upon coordination with a cation. Due to the fast time scale of these techniques, separate peaks are observed for coordinated vs uncoordinated solvents and anions. Deconvoluting coordinated vs uncoordinated vibrational modes

allows for determination of average coordination numbers of solvents and anions to a cation. Both methods have been used extensively in Li electrolyte literature—and to a lesser degree with other ion chemistries—to develop a qualitative ranking of anion and solvent coordination strengths with Li^+, and to understand Li^+ coordination preferences and aggregation tendencies.

For example, Raman investigation of several Li salts in ACN,[33] as well as FTIR investigation in PC and DMC,[34] have resulted in the following ranking of anion dissociation ability: $PF_6 > FSI > TFSI \geq ClO_4 > BF_4$, where PF_6 is the most highly dissociating anion out of the studied Li salts. Similarly, Raman and FTIR have been used to observe preferences in solvent coordination such as a preference for cyclic carbonates like PC or EC to coordinate to Li^+ over linear carbonates like DMC or DEC.[35, 36] In most Raman and FTIR studies, Li^+ is shown to have a coordination number of 3-5 in nonaqueous organic solvents at dilute concentrations and when monodentate coordination dominates. This is true for carbonates which coordinate through a single carbonyl oxygen, whereas some linear ethers (glymes) can coordinate through multiple ether oxygens from the same molecule, reducing the observed coordination number. It is generally assumed that only the solvent molecules in the first coordination sphere undergo significant changes in their vibrational modes, and that the solvent molecules in the outer coordination spheres, although still existing, don't interact strongly with the cation, and thus are indistinguishable from the bulk solvent in these methods. As salt concentration increases, ion pairs are more likely to form and the smaller ratio of solvent to Li^+ allows for aggregates to form. CIP and aggregation also tend to significantly change the vibrational modes of the anion, and thus researchers have used both Raman and FTIR to study the aggregation of Li^+ and anions at high salt concentrations. It has been especially useful in the development of Locally Highly Concentrated Electrolytes (LHCEs) in which the formation of CIPs is promoted without forming aggregates that are too bulky.[37]

NMR is another nondestructive spectroscopic technique that has been used in the Li battery field but has a time scale slower than the exchange of solvents and anions in the coordination shell of the cation. Thus, instead of observing two separate peaks for coordinated vs uncoordinated molecules, there is a single weighted average peak between where the separate peaks would be. Because of this, it is more challenging to obtain quantitative information about the coordination shell composition. Interestingly, NMR typically results in higher reported coordination numbers. This is because NMR appears to also be sensitive to coordination of solvent molecules in the second coordination shell.[30] Despite the challenges, the advantage of NMR is the ability to identify how coordination affects specific atoms in a molecule. ^{6,7}Li, ^{13}C, and ^{17}O NMR are most commonly used in the Li battery electrolyte field, as these are typically the atoms most involved in coordination. ^{7}Li NMR, for example, has been used in several studies to assess coordination preferences and tendencies.[38, 39] And ^{13}C and ^{17}O NMR have been used to quantify coordination numbers of solvents to Li^+.[30, 35, 38]

Some groups have also used a soft ionization technique, ESI-MS, to probe the coordination shell composition.[3, 40] Unlike the other spectroscopic techniques mentioned here, ESI-MS is destructive. It subjects the electrolyte to a high voltage to create an aerosol. The principle behind the use of ESI-MS for electrolytes is that only the strongest interactions with the cation—the first coordination shell—will remain intact upon ionization, and thus the cation and first coordination shell complex can be analyzed via mass spectroscopy.

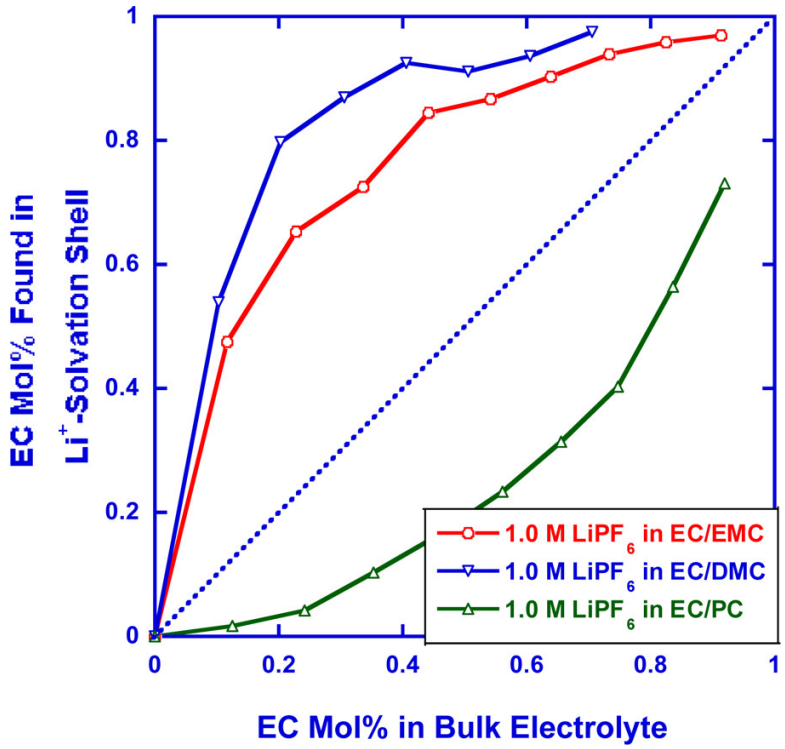

Figure I.4: ***Preferential solvation of Li^+ revealed by electrospray ionization mass spectroscopy.*** *Preferential solvation of Li^+ in EC:PC, EC:DMC, and EC:DMC mixtures. The dashed line is a guide for non-preferential solvation. Figure reproduces from A.W. Cresce, et al.* J. Phys. Chem. C ***2012***.[3]

ESI-MS was used to investigate a 1 M $LiPF_6$ in EC:PC electrolyte with varying mole fractions of EC in the bulk electrolyte.[3] As shown in Figure I.4, PC was found to be the preferred solvent in the first Li^+ coordination sphere in the gas phase. This is compared to solvent mixtures of EC:EMC and EC:DMC in which the cyclic carbonate EC is known to preferentially solvate Li^+ over the linear carbonates as mentioned previously. It is noted that this result contradicts previous spectroscopic studies which found no preference between EC and PC,[41] and computational studies which calculated a slight preference for EC over PC.[42] The inconsistency across these different techniques highlights a lack of understanding of the mechanisms and driving forces for solvent coordination in these electrolytes.

I.3.2. Computational Approaches

Lastly, density functional theory (DFT) and molecular dynamics (MD) are both powerful computational approaches to attaining a deeper understanding of the electrolyte coordination environment. In fact, nearly all the spectroscopic studies referenced above utilize at least one of these computational methods to corroborate and better interpret the spectroscopic results. High accuracy DFT simulations come with a very high computational cost. Thus, most researchers opt to use hybrid DFT functionals like B3LYP, or simulate the electrolyte with MD. These methods are less computationally expensive without sacrificing too much accuracy, but it is important to recognize that the choice of the DFT functional/basis set or the MD force field can significantly change the equilibrium energies, and as such can affect the interpretation of the electrolyte coordination environment.

I.4. Ion Solvation and Complexation Thermodynamics

While the spectroscopic and computational approaches to investigating the cation coordination shell are powerful and insightful, they lack quantitative means to compare binding compositions and strengths across several electrolytes. Inconsistencies in spectroscopic approaches, spectral deconvolution, DFT functionals, and MD force fields all contribute to difficulties in comparing the coordination environment between several electrolytes and studies. From this emerges a clear need for a quantitative metric that enables comparison and, more importantly, prediction of coordination shell properties. One such set of metrics is the thermochemical properties of coordination: Gibbs free energy, enthalpy, and entropy.

Measuring the Gibbs free energy, enthalpy, and entropy of coordination in solution is a problem that has been addressed extensively in literature; however, these studies primarily examine the formation and properties of complexing between ligands and receptors in the biochemical and pharmaceutical fields, and not on complexing between solvents and cations. On the other hand, solvent-solute interactions have been studied extensively in electrochemical literature, but focus primarily on measuring the Gibbs free energy, enthalpy, and entropy of *solvation*, which differs from cation complexation thermodynamics in that it also captures breaking of the salt lattice and disruption of solvent-solvent interactions. Despite their similarities, only a few studies, to the author's knowledge, have attempted to bridge the gap between metal complexation thermodynamics and solvation thermodynamics to measure individual solvent coordination thermodynamics to a cation in the nonaqueous electrochemistry field.

I.4.1. Thermodynamics of Ion Solution

The thermodynamics of ion solution refers to the energy changes involved with the dissolution of a salt in a solvent. Dissolution of a salt is a complex process which can be thought of as occurring through three main processes. (1) The ionic interactions that bind the salt lattice are broken apart so that they

are not interacting (solid to gas phase). This lattice-breaking process is endothermic and results in an increase in entropy with respect to the ordered lattice ($\Delta H_{lat} > 0,\ \Delta S_{lat} > 0$). (2) The solvent-solvent interactions are disrupted to make a cavity for the solute. Once again, this process is endothermic and increases entropy with respect to the ordered solvent ($\Delta H_{cav} > 0,\ \Delta S_{cav} > 0$). (3) The solute is then inserted into the cavity and the solvent coordinates with the ions. This process is exothermic and typically reduces entropy of the solvent-salt system ($\Delta H_{coord} < 0,\ \Delta S_{coord} < 0$). It is important to note that other interactions beyond direct coordination arise, such as ion-ion and ion-dipole forces, but in this framework, we will lump them with the coordination process. The total enthalpy of and entropy of solution are then $\Delta_{sol}H = \Delta H_{lat} + \Delta H_{cav} + \Delta H_{coord}$ and $\Delta_{sol}S = \Delta S_{lat} + \Delta S_{cav} + \Delta S_{coord}$. Thus, the sign and magnitude of the free energy change of solution, $\Delta_{sol}G = \Delta_{sol}H - T\Delta_{sol}S$, is dependent on the extent to which ΔH_{coord} and ΔS_{coord} compensate for endothermic and entropically favorable lattice-breaking and solvent cavity formation. Unfortunately, it is impossible to experimentally isolate and measure each process directly, thus we can only infer how these processes compete based on the experimentally attainable values of $\Delta_{sol}G$, $\Delta_{sol}H$, and $\Delta_{sol}S$. Further discussion on what can be inferred from $\Delta_{sol}H$ measurements is provided in the results (Sec. III.1)

Copious amounts of standard $\Delta_{sol}G^{\infty}$, $\Delta_{sol}H^{\infty}$, and $\Delta_{sol}S^{\infty}$ values have been reported in literature for a wide range of salts and solvents, especially for aqueous solutions and others relevant to biology. In this context, standard thermochemical values are reported 25 °C and 'infinite' dilution, at which ions are fully dissociated and do not interact with each other. 'Infinite' dilution is approximated by very dilute solutions, extrapolation from concentration dependence curves, or computation. Over the past century, many experimental techniques have evolved such that it would be infeasible to cover all the methods used to obtain these values. Instead, a single, common method for the measurement of each $\Delta_{sol}G$ and $\Delta_{sol}H$ are provided for the reader to better understand how these values are obtained.

The Gibbs free energy of solution, $\Delta_{\mathrm{sol}}\mathrm{G}$, is widely measured via solubility experiments to obtain the solubility product, $\mathrm{K_{sp}}$, for the dissolution reaction:

$$\mathrm{AB\ (solid)} \rightleftharpoons a\mathrm{A^{+}\ (solv.)} + b\mathrm{B^{-}\ (solv.)}$$

$$\mathrm{K_{sp}} = [\mathrm{A^{+}}]^{a}\,[\mathrm{B^{-}}]^{b}$$

where $[\mathrm{A^{+}}]$ is the equilibrium concentration of the cation in solution and $[\mathrm{B^{-}}]$ is the equilibrium concentration of the anion in solution. The equilibrium concentration of ions in a saturated solution is typically detected via spectroscopic methods or potentiometric methods. Then, the Gibbs free energy of solution can be calculated via

$$\Delta_{\mathrm{sol}}\mathrm{G} = -\mathrm{RT}\ln\left(\mathrm{K_{sp}}\gamma_{\pm}^{(a+b)}\right)$$

where $\gamma_{\pm}$ is the mean ionic activity coefficient. $\gamma_{\pm}$ describes the deviation of the cation and anion from their ideal behavior and is a function of ion charges and the concentration of ions. It can be determined experimentally or via a semi-empirical relationship such as the Davies equation.[43] This method, however, works best for sparingly soluble salts because $\gamma^{\pm}$ is not easily obtained at high concentrations, and other experimental techniques or computation are needed to get $\Delta_{\mathrm{sol}}\mathrm{G}$ at concentrations which can approximate 'infinite' dilution for highly soluble salts.

Measurement of $\Delta_{\mathrm{sol}}\mathrm{H}$ is relatively straightforward and can be simply obtained with a calorimeter by measuring the heat released/absorbed upon dissolution of the salt in a solvent. Conventionally, this measurement is carried out by preparing a glass ampoule filled with salt, submerging it in the solvent, and breaking the ampoule inside the calorimeter reaction chamber. These experiments are typically performed at very dilute concentrations ($\lesssim 0.01\ \mathrm{M}$) to approximate an 'infinitely' dilute solution. With both $\Delta_{\mathrm{sol}}\mathrm{H}$ and $\Delta_{\mathrm{sol}}\mathrm{G}$ at the same experimental conditions, it is then trivial to calculate $\Delta_{\mathrm{sol}}\mathrm{S}$.

A thorough review of ion solvation in aqueous and non-aqueous electrolytes, as well as tables of solution thermodynamics is provided by Y. Marcus in "Ions in Solution and their Solvation."[44] Despite the large databases on ion solvation thermodynamics, there is a lack of thermochemical solvation information on more modern, battery-relevant salts (e.g $LiPF_6$, LiTFSI) and solvents (e.g. FEC, DME).

I.4.2. Thermodynamics of Ion Transfer

Having established the solution thermodynamics of many salts going from the solid phase to the solution phase, researchers became interested in bypassing the challenges associated with the ill-defined transfer between phases. Instead, it would be easier to study the transfer of ions from a reference solution, in which the solution thermodynamics are well understood, into a solvent of interest. Historically, water is chosen as the reference solvent because the solution thermodynamics and solvation structure have been investigated the most rigorously. This is a clever approach because it largely circumvents the unknown energies involved with lattice breaking and cavity formation and, as will be discussed in a moment, allows for direct and more accurate measurement of free energies of transfer at dilute concentrations without extraneous assumptions about ion activities. Transfer thermodynamics can be described as the difference in solution thermodynamics between the solvent of interest (S) and the reference solvent (R):

$$\Delta_{\mathrm{tr}}\mathrm{Y}(\mathrm{salt}, \mathrm{R} \rightarrow \mathrm{S}) = \Delta_{\mathrm{sol}}\mathrm{Y}(\mathrm{salt}, \mathrm{S}) - \Delta_{\mathrm{sol}}\mathrm{Y}(\mathrm{salt}, \mathrm{R})$$

where Y, is one of Gibbs free energy (G), enthalpy (H), or entropy (S).

The Gibbs free energy of transfer is primarily measured using solubility, polarographic, or open circuit voltage techniques. Notably, the Gibbs free energy of transfer of the cation, $\Delta_{\mathrm{tr}}\mathrm{G}(\mathrm{C}^+, \mathrm{R} \rightarrow \mathrm{S})$, can be obtained directly via the electromotive force of an electrochemical cell in the form:[45]

Metal Electrode or ISE	Salt in R	Salt Bridge	Salt in S	Metal Electrode or ISE

This allows for the direct and accurate measurement of single cation $\Delta_{tr}G$ without the need for extrathermodynamic assumptions. On the other hand, enthalpies of solution ($\Delta_{sol}H$) remain the most accurate way to attain enthalpies of transfer ($\Delta_{tr}H$), and extrathermodynamic assumptions are required if single ion contributions are desired.

The most widely used extrathermodynamic assumption in this field is the TATB (or TPTB) assumption, which aims to have an anion and cation of equal, spherical size that are non-interacting with the solvent and only differ in the sign of the charge. The tetraphenyl ions Ph_4As^+ (or Ph_4P^+) and Ph_4B^- have been shown to satisfy these conditions relatively well and are widely agreed to provide the most accurate single ion transfer thermodynamics compared to alternative extrathermodynamic assumptions.[46] It is assumed that:

$$\Delta_{tr}Y(Ph_4As^+) = \Delta_{tr}Y(Ph_4B^-)$$

With a series of experiments using the TATB ions with cations and anions of interest, it is possible to isolate single ion thermodynamics of transfer. Once again, there is a lack of data in published literature for more relevant battery ions (particularly anions) and solvents, but some reported battery relevant single-ion transfer thermodynamics from PC to other aprotic solvents are summarized in Table I.1 (single ion enthalpies of transfer) and Table I.2 (single ion Gibbs free energies of transfer). From the data in Table I.1, we observe that the monoatomic monovalent cations, Li^+, Na^+, and Ag^+ are more enthalpically stable in most other polar aprotic solvents than in PC with the exception of Li^+ in SL, which means that the electrostatic interactions between PC and the cations are relatively weak compared to the other investigated solvents. Similarly, in Table I.2 we observe that for Li^+, Na^+, and Ag^+, the free energy decreases upon transfer from PC to all other studied polar aprotic solvents, with the exception of the

transfer of Li^+ into ACN. Therefore, in most cases the transfer from PC to another polar aprotic solvent is both enthalpically and entropically favorable. For anions, on the other hand, the sign of enthalpy and entropies of contribution are less predictable and depend more-so on specific interactions and anion size. Notably, the single ion transfer data for anions is more sparse, and as far as is known here, no thermodynamics of transfer for battery relevant anions such as PF_6^-, $TFSI^-$, or FSI^- have been reported.

Table I.1: ***Single ion standard molar enthalpies of transfer from PC to other polar aprotic solvents,*** $\boldsymbol{\Delta_{tr}H^{\infty}(I^{\pm}, PC \rightarrow S)}$***.*** *Data calculated from standard compilations in Y. Marcus, "Ions in Solution and Their Solvation."*[44]

$\mathbf{\Delta_{tr}H^{\infty}(I^{\pm}, PC \rightarrow S)}$ $\mathbf{(kJ/mol)}$					
Solvent (S) =	**ACN**	**DMF**	**DMA**	**DMSO**	**SL**
Cations					
Li^+	-15.8	-28.2		-30.6	9.2
Na^+	-0.9	-23.6	-28.5	-19.3	-5.5
Ag^+	-41.6	-23.9		-40.4	-2.9
Ph_4As^+	1.0	-4.1	-0.6	1.9	2.1
Anions					
ClO_4^-	-0.3	-7.1	1.0	-2.9	
$CF_3SO_3^-$	0.8			2.1	
F^-		5.7			
Cl^-	-7.8	-4.8	9.4	-6.2	0.8
Br^-	-7.6	-9.7	2.0	-10.5	-2.2
NO_3^-	2.8			-0.5	
Ph_4B^-	1.1	-4.8	-3.3	2.0	2.2

Table I.2: ***Single ion standard molar Gibbs free energies of transfer from PC to other polar aprotic solvents,*** $\boldsymbol{\Delta_{tr}G^{\infty}(I^{\pm}, PC \rightarrow S)}$***.*** *Data calculated from standard compilations in Y. Marcus, "Ions in Solution and Their Solvation."*[44]

	$\mathbf{\Delta_{tr}G^{\infty}(I^{\pm}, PC \rightarrow S)}$ $\mathbf{(kJ/mol)}$							
Solvent (S) =	**Acetone**	**ACN**	**DMF**	**DMA**	**DMSO**	**NMF**	**NMP**	**SL**
Cations								
Li^+	-13.8	4.7	-46.2	-45.8	-41.1	-43.8	-58.8	-17.8
Na^+	-4.6	-2.7	-25.2	-26.7	-27.3	-21.6	-29.6	-17.6
Ag^+	-9.8	-42.9	-36.0	-47.8	-50.8	-33.8	-44.8	-22.8
Ph_4As^+	4.0	1.8	-3.1	-2.7	-2.3		-4.0	0.0
Anions								
ClO_4^-		5.0	7.0		2.0		-9.0	
$CF_3SO_3^-$		-23.0						
F^-		-9.0	-5.0					
Cl^-	17.2	2.3	8.5	15.1	-0.9		11.2	7.2
Br^-	12.0	1.3	6.2	14.0	-5.7		7.0	5.0
NO_3^-		21.0						
Ph_4B^-	4.0	2.4	-2.5	-2.7	-1.1	3.0	-4.0	0.0

I.4.3. Preferential Solvation of Ions

Up until this point, we have only discussed ion solvation in electrolytes with a single solvent. However, in modern battery electrolytes, it is very common to have a mixture of solvents (usually 2-3) along with other additives. In this case, the different solvents/additives will be in competition to enter the primary coordination sphere of the ions, and depending on the energetics of solvent coordination, some solvents may be preferred in the coordination sphere. This is referred to as preferential solvation, or selective solvation, of ions and has been a topic of research for at least the past 5 decades; even still, it is relevant in current LMB research. For example, modern LHCE Li electrolytes are only possible because of preferential coordination of solvent and anions to Li^+ over the diluent.

As discussed earlier, the Li battery field frequently uses a range spectroscopic and computational techniques to investigate the coordination sphere of Li^+. This has enabled the determination of qualitative trends in Li^+ coordination preference, but, to the author's knowledge, hasn't led to any experimental quantitative description of the magnitude of Li^+ coordination preference. This makes it difficult to predict what could be expected in the Li^+ coordination sphere of a new electrolyte without rigorous spectroscopic study or computationally expensive simulation.

It is, however, possible to quantify the degree of selective coordination with any experimentally accessible quantity which is linearly dependent on the composition of the coordination sphere. There are a handful of models/metrics which have been used to enable this quantification.[47-50] In the context of this work, a stepwise solvation exchange model is the most relevant and quantifies the degree of preferential solvation with an average equilibrium constant, $\mathrm{K_{PS}}$.[48] This model will be discussed at length in Section II.4, but for now it is sufficient to know that this value essentially quantifies the change in Gibbs free energy when the solvents are mixed in the coordination sphere. A $\mathrm{K_{PS}} = 1$ would indicate that there is no preference for either solvent (i.e. the free energy does not change with mixed solvents) and a $\mathrm{K_{PS}} \neq 1$ indicates that there is selective coordination with the ion (i.e. the free energy increases or decreases as solvents are mixed in the coordination sphere). Thermodynamics of transfer[51, 52] and spectroscopically attainable values such as NMR chemical shifts[39, 53-56] can both be used to calculate $\mathrm{K_{PS}}$.

For example, by measuring $\Delta_{\mathrm{tr}}\mathrm{Y}(\mathrm{R} \rightarrow \mathrm{S})$ from a neat solvent to a binary mixture of solvents for a range of compositions, one can construct a curve $\Delta_{\mathrm{tr}}\mathrm{Y}(\mathrm{R} \rightarrow \mathrm{S}) = f(X_{mix})$, where X_{mix} is a mole fraction that quantifies the mixture composition, of which the curvature, inflections points, and extrema can provide insight into preferential solvation and complexation.[51, 52, 57-59] Fitting the curve to a model allows for extraction of $\mathrm{K_{PS}}$. Similarly, it is possible to construct a curve of NMR chemical shifts as a function of mixture composition and extract $\mathrm{K_{PS}}$ with a model. While this is a useful technique to understand

driving forces for solvation of ions it lacks the ability to isolate single solvent-ion interaction energies. One possible way to isolate single solvent-ion coordination thermodynamic is by using techniques developed for the study of metal ion complexation chemistry.

I.4.4. Ion Complexation

A complex ion is a species formed by the association of a central metal ion with one or more surrounding ligands, and the resulting structure is called a coordination complex. The study of ion complexation developed in parallel with the study ion solution/transfer thermodynamics; however, despite their striking similarities, there has been little overlap in the application of complexation chemistry techniques to the study of ion solvation. A general approach for the measurement of metal complexation thermodynamics was first established by Jannik Bjerrum in 1941. In his thesis, he developed a general method for the determination of stability constants of metal-amine complexes in aqueous solution using a pH meter to measure the proton concentration throughout the course of a titration.[60] The stability constant, β_i, was defined by applying the law of mass action to the following reaction:

$$\mathrm{M} + \mathrm{iL} \rightleftharpoons \mathrm{ML_i}$$

$$\beta_\mathrm{i} = \frac{[\mathrm{ML_i}]}{[\mathrm{M}][\mathrm{L}]^\mathrm{i}}$$

where [M] is the equilibrium concentration of the free metal ion, [L] is the equilibrium concentration of the free ligand, and $[ML_i]$ is the equilibrium concentration of the metal-ligand complex. Bjerrum's work led to the widespread documentation of stability constants in volumes and digital databases, with potentiometric titration methods becoming the standard for such determinations. However, there are now several alternative methods including NMR, spectrophotometric, or calorimetric titrations; to name the most popular. A majority of the complex equilibria studies focus on aqueous systems and biological

ligands like amino acids. Only a small fraction study the coordination of nonaqueous solvent molecules to ions.

For example, K. Izutso, et al. (1974) examined the complexing of sodium ions in acetonitrile with other solvents.[61] They used an electrochemical cell with a Ag/Ag^+ reference electrode, a monovalent cation sensitive glass electrode, and a salt bridge to determine the change in chemical potential of Na^+ in ACN as a second solvent, S, is titrated into the electrolyte:

$$\mathrm{Ag}\left|\begin{matrix}5\mathrm{mM\ AgNO_3}\\(\mathrm{ACN})\end{matrix}\right\|\begin{matrix}0.1\mathrm{M\ Et_4NPi}\\(\mathrm{ACN})\end{matrix}\left\|\begin{matrix}1\mathrm{mM\ NaClO_4}+0.01\mathrm{M\ Et_4NClO_4}\\(\mathrm{ACN}+\mathrm{S})\end{matrix}\right|\begin{matrix}\text{monovalent cation sensitive}\\\text{glass electrode}\end{matrix}$$

The emf of the cell is then related to the change in free energy of Na^+ by $\Delta G_{Na^+} = -zFE_{cell}$, where F is the Faraday constant and z is the number of electrons involved in charge transfer ($z = 1$ for Na^+). Following Bjerrum's model formalism, they calculated the stability constants, β_i, of the complexes formed with addition of water, methanol, DMF, DMA, DMSO, and hexamethylphosphoramide (HMPA). They found that all the examined solvents except methanol preferentially solvated Na^+ over ACN, and can quantitatively describe the free energy of stepwise formation of Na complexes. This demonstrates an advantage over previous investigations of preferential solvation discussed in Section I.4.3, in that it quantifies the single solvent-ion interactions that occur as ACN is displaced from the primary coordination sphere. Several similar studies with different cations were carried out.[2, 62-66] Notably, K. Izutsu revisited this technique in 1996 to study the complexation of solvents with Li^+ in some solvents relevant to Li-ion batteries including PC, monoglyme (DME), diglyme, triglyme, DMC, and DEC.[65]

In 1966, Christensen et al. developed a general method for isothermal titration calorimetry (ITC) in which ΔG, ΔH, ΔS and stoichiometry of ligand-receptor complexation could be extracted from a single experiment.[67] The method essentially utilizes J. Bjerrum's complexation titrations with calorimetry instead of potentiometry. Modern ITC is commonly used in biology to measure the strength of biological

ligands binding with macromolecules and is especially important in quantifying the effectiveness of drugs in binding to specific proteins in the body. It involves the titration of small amounts of a ligand into a solution containing the macromolecule and measuring the heat generated or absorbed due to binding after each injection. As this is a calorimetric experiment, it is important to remember that the measurement includes the heat of all reactions occurring during titration. To isolate the binding enthalpy, control experiments are typically conducted to subtract other heats:

$$\Delta H_{\text{binding}} = \Delta H_{\text{measured}} - \Delta H_{\text{dilution of ligand}} - \Delta H_{\text{dilution of receptor}}$$

$\Delta H_{\text{measured}}$ is the heat measured when injecting a pH buffered solution containing the ligand into an identically buffered solution containing the macromolecule receptor. The importance of the pH buffer is a consequence of the strong pH and salt concentration dependence of biological systems. $\Delta H_{\text{dilution of ligand}}$ is the heat measured when injecting the buffered ligand solution into a pure buffer solution. And similarly, $\Delta H_{\text{dilution of receptor}}$ is the heat measured when injecting a pure buffer solution into the buffered macromolecule solution. $\Delta H_{\text{dilution of receptor}}$ is often ignored because the injection volumes are often much smaller than the receptor solution volume, resulting in negligible dilution heats.

The heat per injection typically results in a sigmoidal curve shape as shown in Figure I.5. This is because with each initial injection, all of the newly introduced ligand binds to a macromolecule, releasing around the same amount of heat per injection up until the point where all macromolecules are bound to a ligand, and the heat per injection quickly drops off towards zero. Some key geometric features of this sigmoidal share are the amplitude, which corresponds to the enthalpy of coordination; the inflection point location along the x-axis, which gives the stoichiometry of the coordination; and the steepness of the curve, which is related to the binding affinity of ligand to the macromolecule.[68, 69] The ITC curve is commonly fit to a binding model, similar to Bjerrum's, to extract these values.[70, 71]

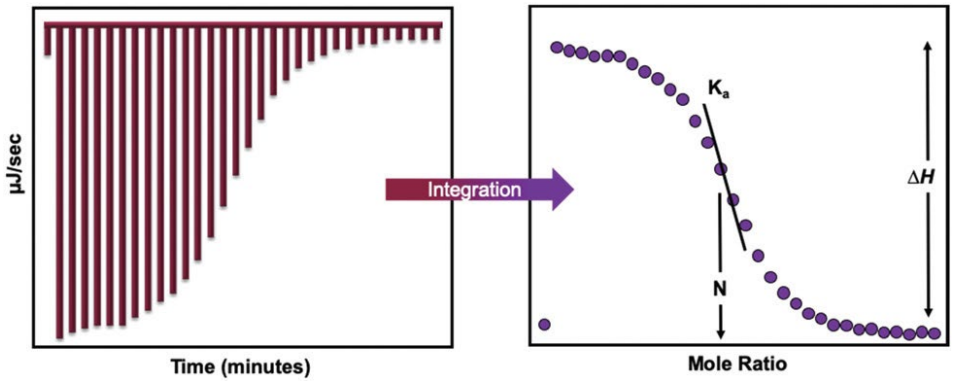

Figure I.5: ***Typical ITC thermogram and curve shape.*** *Each peak of the microcalorimeter thermogram (left) is a result of a single injection. The heat of each injection is obtained by integration of each peak and produces an ITC curve (right). The isotherm is dependent on the association constant (K_a), change in enthalpy (ΔH), and the stoichiometry (N) of the association reaction under investigation. Figure is reproduced from W. Archer and M. Schulz,* Soft Matter **2020**.[69]

Despite the powerful ITC technique being used for over 50 years in the biochemical field, it has not, to our knowledge, been used to quantify the thermochemical driving forces behind solvent-ion coordination. Using both ITC and potentiometric titrations to quantify solvent-ion coordination thermodynamics may be pivotal in understanding SEI formation pathways and unlocking new design principles to reach highly efficient batteries with Li and beyond-Li anode chemistries.

I.5. Thesis Objectives

The research objectives of this thesis are to: (1) review and supplement literature on the thermodynamics of Li battery electrolyte solvation environments, (2) develop the use of calorimetric and potentiometric titrations as a method for determination of ion-solvent complex thermodynamics, and (3) to apply and assess the validity of this method on select, well-studied Li electrolytes.

The first objective is timely because much of recent LMB research has focused on electrolyte design as a handle for fine-tuning SEI properties, yet fundamental studies of ion solvation thermodynamics have scarcely been brought into the context of the Li battery field. This is a largely untapped collection of data, knowledge, and experimental techniques which could potentially be used to accelerate and optimize the electrolyte design process for Li electrolytes and beyond. Much of the review portion of this objective has been met above (Section I.4) in the review of thermodynamics of solution and transfer. In the first section of the results, we use a microcalorimeter to supplement literature with enthalpies of solution and enthalpies of transfer for the Li-battery relevant salts LiTFSI and $LiPF_6$ in a range of polar aprotic solvents. While these measurements provide valuable insight into relative cation/anion solvating ability of these solvents, they lack the microscopic ion-solvent coordination fidelity that would enable researchers to predict the coordination environment of new electrolyte blends. To achieve this fidelity, we chose to adapt titration techniques from the complexation chemistry field.

The second section of this study focuses on the development of calorimetric (ITC) and potentiometric (PT) titration methods to measure the Gibbs free energy, enthalpy, and entropy of solvent displacement in the coordination sphere of a cation. As with any calorimetric method, ITC measures the heat of all reactions that occur in the cell. This necessitates rigorous investigation of the interactions which evolve through the course of the titrations to ensure proper isolation of cation-solvent interactions.

Potentiometric titrations, on the other hand, require careful cell configuration in order to minimize error from liquid junction potentials. Following the verification of experimental methods, we adapted a statistical stepwise solvent replacement model and a data fitting procedure which can be used to obtain the desired thermochemical properties of the reaction.

Lastly, the third section of the study aims to validate the method and model by applying them to a set of Li electrolytes which have been studied in the battery field via other spectroscopic and computational methods. This lays the foundation for deeper studies into more complex systems. First, we examine an EC:DMC electrolyte in which there is a well-known preference for EC in the coordination sphere of Li^+. This confirms that our method agrees with literature. We then chose to examine an EC:PC electrolyte in which there are differing conclusions, as discussed above, to whether EC or PC is preferred in the Li^+ coordination sphere and to what degree. Overall, this thesis brings past study of ion solvation thermodynamics into the context of battery electrolytes, specifically Li battery electrolytes, and implements ITC and PT techniques, which are novel to the battery field, to obtain new insight and predictive capabilities in the formation of cation-solvent complexes.

Note that this study is focused on Li electrolyte solvation because it is the most well-understood of the battery relevant metals; however, the techniques are being developed with the goal of further application to other cations with more complex solvation environments. For example, Ca^{2+} represents an extreme case of alternative battery electrolyte metal ions, whereby the low charge density and high polarizability of Ca^{2+} afford coordination numbers of 7-9. In principle, the large coordination numbers allow for greater flexibility and customization of the coordination sphere, however researchers have not yet learned how to exploit this as a design variable. This work aims to provide a different perspective and new tools to design optimal battery electrolytes for any battery chemistry.

II. Experimental Methods

II.1. Materials

All materials were stored and handled in an Ar glovebox (H_2O content < 0.1 ppm, O_2 content < 0.1 ppm, MBRAUN). All solvents were used as received. Li salts were vacuum dried in a Buchi oven at 120 °C for at least 24 hours. All other salts were used as received.

Name	Supplier	Purity (%)
Solvent		
ACN	Sigma Aldrich	99.8 (anhydrous)
DEC	Sigma Aldrich	99 (anhydrous)
DMA	Sigma Aldrich	99.8 (anhydrous)
DMC	Sigma Aldrich	99 (anhydrous)
DME	Sigma Aldrich	99.5 (anhydrous, inhibitor-free)
DMF	Sigma Aldrich	99.8 (anhydrous)
DMSO	Sigma Aldrich	99.9 (anhydrous)
DOL	Sigma Aldrich	99.8 (anhydrous, inhibitor)
EC	Acros Organics	99
MeTHF	Sigma Aldrich	99 (anhydrous, inhibitor-free)
PC	Sigma Aldrich	99.7 (anhydrous)
SL	Sigma Aldrich	99
THF	Sigma Aldrich	99.9 (anhydrous, inhibitor)
Salt		
$LiPF_6$	Sigma Aldrich	99.99 (battery grade)
LiTFSI	Sigma Aldrich	99.99 (anhydrous)
$LiClO_4$	Sigma Aldrich	99.99 (battery grade, dry)
LiFSI	Arkema	99.9
$TBAClO_4$	Sigma Aldrich	98
$TBAPF_6$	Sigma Aldrich	99
TBATFSI	Ambeed	97
Ph_4PI	Ambeed	95
$NaPh_4B$	Ambeed	98
NaI	Thermo Scientific	99
NaTFSI	Sigma Aldrich	97

II.2. Microcalorimetry

Microcalorimetry experiments were performed using a Thermal Hazard Technologies Micro Reaction Calorimeter (μRC). Electrolyte samples were placed in sealed glass vials in an Ar glovebox. Two vials were prepared for each experiment, one for the reaction under investigation, and one for a reference. For isothermal solid addition experiments, the dry salts were prepared and sealed into the injection apparatus in the glove box. The salts were manually injected with a Teflon plunger after thermal stabilization. For isothermal titration experiments, a glass syringe was prepared with the injectant in the glove box and the sample was sealed with a septum. Injections were automated with the μRC; the equipment ensures thermal stabilization before each subsequent injection. All μRC experiments were stirred with a Teflon stir bar at 200 rpm and were conducted isothermally at 25 °C unless stated otherwise.

II.3. Potentiometry

All potentiometry experiments were conducted within an Ar glovebox. A glass three-electrode cell (Pine Research, Low Volume Cell) was used for electrochemical measurements, and setup with symmetric Li electrodes, and asymmetric electrolytes as described in Ref.[20] A Li/Li^+ reference electrode was prepared, and a salt bridge (1 M LiTFSI DOL:DME (1:1 v/v)) was used to minimize the liquid junction potential between the reference and sample solution. The reference electrode electrolyte, salt bridge electrolyte, and sample electrolyte were all separated by glass frits using a double-junction reference electrode chamber (Bioanalytical Systems, Inc.). A fresh Li metal working electrode was rolled, polished, and affixed in a stainless steel holder to be submerged in the electrolyte. Titrations were performed with a pipette through an opening in the cell cap. The cell OCV was monitored using a Bio-Logic potentiostat.

II.4. Raman Spectroscopy

Electrolyte samples were sealed in glass vials under Argon atmosphere in the glove box. Raman spectroscopy was performed on the sealed samples using a Renishaw inVia Confocal Raman Microscope. A 532nm 50mW laser was used with a 2400 lines/mm reflectance grating. Several accumulations were collected to improve the signal-to-noise ratio of the spectra. Raman spectra were first baseline corrected, then areas of interest were deconvoluted using Pseudo-Voigt profiles.

III. Results & Modeling

III.1. Enthalpy of Solution

Microcalorimetric measurements were conducted to measure the solution enthalpy of $LiPF_6$ and LiTFSI in a range of polar aprotic solvents. We used a solid addition setup in which a salt is pushed into the sample vial with a plunger (Figure III.1). The salt is held above the sample with a thin PTFE stopper, which is dislodged when enough force is applied to the plunger, and the salt is then dissolved in the solvent with stirring.

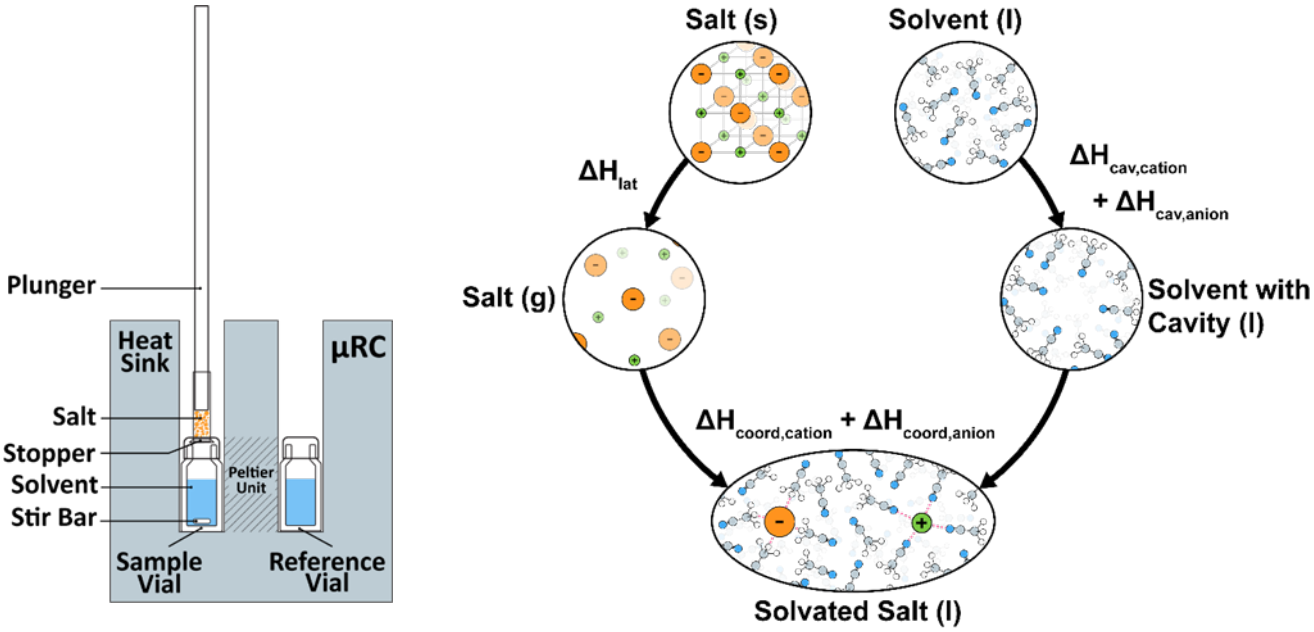

Figure III.1: ***Enthalpy of solution microcalorimetry setup, and a schematic of the contributions to the heat released/absorbed during dissolution.*** *On the left is a diagram of the power compensation microcalorimeter (μRC) apparatus with plunger for the addition of salt into the sample vial. On the right, an illustration of the processes that occur during salt dissolution including lattice breaking, solvent cavity formation, and ion-solvent coordination.*

It is important to note that calorimeters measure the combination of all the heat released or absorbed by a reaction. As such, we must consider what we are really probing in a solution enthalpy measurement. As discussed in Section 1.4.1, the dissolution of a salt can be broken down into three

main contributions, summarized in Figure III.1. First, the lattice of the salt must be broken. The lattice enthalpy, $\Delta_{\mathrm{lat}}\mathrm{H}$, is defined as the heat required to break apart the lattice into gaseous ions, so far apart that there is negligible interaction between ions. This is a strongly endothermic contribution to the solution enthalpy. Second, the solvent must reorganize and form a cavity large enough for a cation or anion to be inserted. The cavity formation enthalpies, $\Delta_{\mathrm{cav}}\mathrm{H}$, are significantly endothermic as it requires work to pull the solvent molecules apart. Last, the gaseous ions can be inserted into the solvent cavities, and solvent molecules strongly interact or coordinate with the ions. The coordination enthalpies ($\Delta_{\mathrm{coord}}\mathrm{H}$)—also known as solvation enthalpies or hydration enthalpies in the case of water—are strongly exothermic contributions to the solution enthalpy. So much so, that all the solution enthalpies measured with $LiPF_6$ and LiTFSI in the selected solvents are exothermic (Figure III.2).

All solution enthalpy experiments were conducted at 25 °C with 1 mL of solvent in the sample vial, and the amount of salt dissolved was adjusted such that the final solution had a molar concentration of 0.1 M of either $LiPF_6$ or LiTFSI. While the small volume of the sample vial in our μRC is beneficial for quick and accurate power compensation, it makes it difficult to reach concentrations which are typically used to approximate 'infinite' dilution ($\lesssim 10\ \mathrm{mM}$). For example, to achieve 0.1 M $LiPF_6$ for 1 mL of solution, we use 15.2 ± 0.1 mg of $LiPF_6$, which is approaching the limit of how much salt we can accurately weigh and dispense in our apparatus. Furthermore, with very small masses of salt, there is proportionately less heat released/absorbed, and measurements are more prone to noise errors. The concentration dependence of $\Delta_{\mathrm{sol}}\mathrm{H(LiTFSI)}$ in PC was evaluated from 0.025 M to 0.2 M and we found that at concentrations ≤ 0.1 M the $\Delta_{\mathrm{sol}}\mathrm{H(LiTFSI)}$ was unchanging within 1 kJ/mol (Figure A.1), thus 0.1 M LiTFSI in PC is at approximately 'infinite' dilution. However, PC has the highest dielectric constant of all solvents we examined (66.1). For solvents with lower dielectric constants like DEC (2.82), 0.1 M is likely too concentrated to approximate infinite dilution with these salts. This is okay for the purposes of our

study as long as we consider its effect in our discussion of trends, but these values cannot be used in the same way as one would use a standard molar enthalpy of solution at 'infinite' dilution.

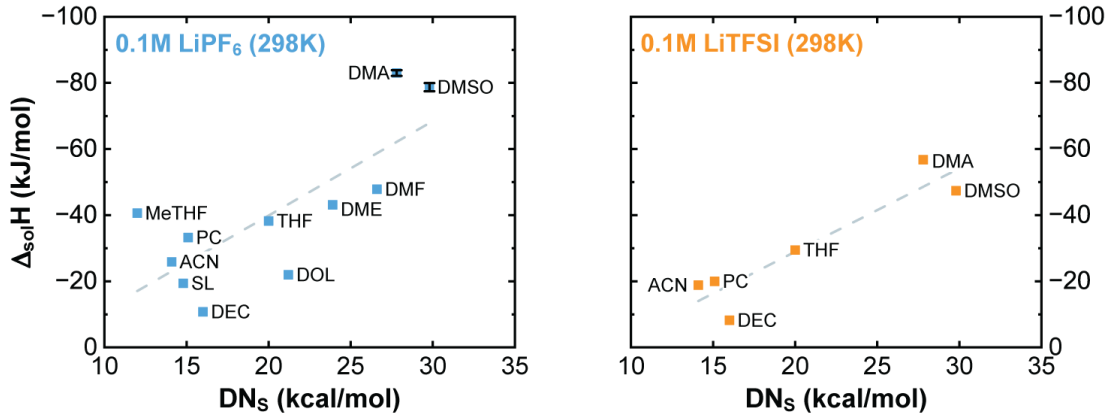

Figure III.2: ***Enthalpies of solution of $LiPF_6$ and LiTFSI in several aprotic solvents vs solvent donor number (DN).*** *The dashed line highlights a general trend that increasing solvent DN is correlated with increasing $\Delta_{sol}H$.*

With that in mind, we can examine the measured enthalpies of solution shown in Figure III.2. The $\Delta_{\mathrm{sol}}\mathrm{H}$ are plotted vs. the solvent donor number (DN_S) to highlight the qualitative trend that with increasing solvent electron pair donor ability, the enthalpy of solution becomes more exothermic. This is a direct result of stronger cation-solvent interactions which make the $\Delta\mathrm{H}_{\mathrm{coord,cation}}$ contribution more negative. Similarly, we can plot the $\Delta_{\mathrm{sol}}\mathrm{H}$ vs. the solvent acceptor number (AN), but we observe no trend with the solvent Lewis acidity (Figure A.2), suggesting that the solvent interaction with the cation is the dominant contributor (i.e. $\Delta\mathrm{H}_{\mathrm{coord,cation}} \gg \Delta\mathrm{H}_{\mathrm{coord,anions}}$). However, the large vertical scatter observed for solvents with similar DN (e.g. $LiPF_6$ in DEC, SL, ACN, PC, MeTHF) makes it clear that the solvent donicity cannot fully describe the $\Delta_{\mathrm{sol}}\mathrm{H}$, and the scatter is, at least in part, due to the solvent-anion interactions. Additionally, for solvents with low dielectric constants (DEC, DME, DOL, MeTHF), the measured $\Delta_{\mathrm{sol}}\mathrm{H}$ is likely less negative than $\Delta_{\mathrm{sol}}\mathrm{H}^{\infty}$ because the ion pairs are not fully separated (an endothermic process).

For both $LiPF_6$ and LiTFSI, DMA and DMSO appear to be the most strongly solvating solvents, and DEC appears to be the weakest.

Between $LiPF_6$ and LiTFSI, we observe the same qualitative ranking of $\Delta_{\mathrm{sol}}\mathrm{H}$, however the $\Delta_{\mathrm{sol}}\mathrm{H}(\mathrm{LiTFSI})$ are consistently less exothermic than $\Delta_{\mathrm{sol}}\mathrm{H}(\mathrm{LiPF_6})$. This is due in part to the difference in lattice enthalpies of the salts, suggesting that $\Delta\mathrm{H}_{\mathrm{lat}}(\mathrm{LiPF_6}) < \Delta\mathrm{H}_{\mathrm{lat}}(\mathrm{LiTFSI})$. However, these lattice energies have not been reported in literature, so we are unable confirm this relation. Regardless, we know that that the difference in lattice energies cannot be the only factor that contributes to the difference between $\Delta_{\mathrm{sol}}\mathrm{H}(\mathrm{LiTFSI})$ and $\Delta_{\mathrm{sol}}\mathrm{H}(\mathrm{LiPF_6})$. If that were the case, we would expect all measured $\Delta_{\mathrm{sol}}\mathrm{H}$ to be shifted by a constant amount equal to that $\Delta\mathrm{H}_{\mathrm{lat}}(\mathrm{LiPF_6}) - \Delta\mathrm{H}_{\mathrm{lat}}(\mathrm{LiTFSI})$ across LiTFSI and $LiPF_6$ (assuming full dissociation). Instead, we see that in low DN solvents $\Delta_{\mathrm{sol}}\mathrm{H}(\mathrm{LiTFSI})$ are around 10 kJ/mol less than $\Delta_{\mathrm{sol}}\mathrm{H}(\mathrm{LiPF_6})$, while in high DN solvents $\Delta_{\mathrm{sol}}\mathrm{H}(\mathrm{LiTFSI})$ are around 30 kJ/mol less than $\Delta_{\mathrm{sol}}\mathrm{H}(\mathrm{LiPF_6})$. This is more easily stated as the slope of the qualitative trendline being smaller for LiTFSI. If we assume that the electrolytes are near 'infinite' dilution (which is valid for the high dielectric constant solvents PC, DMSO, DMA, and maybe ACN), then $\Delta\mathrm{H}_{\mathrm{cav,Li^+}}$ and $\Delta\mathrm{H}_{\mathrm{coord,Li^+}}$ are constant for given solvent. Thus, the difference in slope must be due to differences in $\Delta\mathrm{H}_{\mathrm{cav,anion}}$ and $\Delta\mathrm{H}_{\mathrm{coord,anion}}$. Unfortunately, it is impossible to isolate the cavity formation and coordination contributions, so the only concrete conclusion that we can make with this data is $\Delta\mathrm{H}_{\mathrm{cav,TFSI^-}} + \Delta\mathrm{H}_{\mathrm{coord,TFSI^-}} > \Delta\mathrm{H}_{\mathrm{cav,PF_6^-}} + \Delta\mathrm{H}_{\mathrm{coord,PF_6^-}}$. However, it has been shown via PM7-MD simulations that the fluorinated anions PF_6^- and BF_4^- exist largely without solvation due to the lack of a coordination site on polar aprotic solvents.[72] Instead, $\Delta\mathrm{H}_{\mathrm{coord,anion}}$ are largely composed of weak ion-dipole and dispersion forces. It is also expected that $\Delta\mathrm{H}_{\mathrm{cav,TFSI^-}} > \Delta\mathrm{H}_{\mathrm{cav,PF_6^-}}$ due to the larger ionic radius and non-spherical shape of $TFSI^-$ (0.325 nm) vs. PF_6^- (0.254 nm), which is a likely source of the difference in $\Delta_{\mathrm{sol}}\mathrm{H}$ between the two anions.[73]

To further examine the solution thermodynamics and compare with other salts reported in literature, we calculated the enthalpies of transfer from PC to each solvent:

$$\Delta_{\mathrm{tr}}\mathrm{H}(\mathrm{salt}, \mathrm{PC} \rightarrow \mathrm{S}) = \Delta_{\mathrm{sol}}\mathrm{H}(\mathrm{salt}, \mathrm{S}) - \Delta_{\mathrm{sol}}\mathrm{H}(\mathrm{salt}, \mathrm{PC})$$

In doing so, the lattice energy is canceled out (assuming full dissociation), so $\Delta_{\mathrm{tr}}\mathrm{H}$ is solely a function of the difference in cavity formation enthalpies, $\Delta\mathrm{H}_{\mathrm{cav}}(\mathrm{S}) - \Delta\mathrm{H}_{\mathrm{cav}}(\mathrm{PC})$, and the difference in coordination enthalpies, $\Delta\mathrm{H}_{\mathrm{coord}}(\mathrm{S}) - \Delta\mathrm{H}_{\mathrm{coord}}(\mathrm{PC})$, for the cation and anion. Enthalpies of transfer are convenient because they directly measure the difference in enthalpies between a sample electrolyte and reference

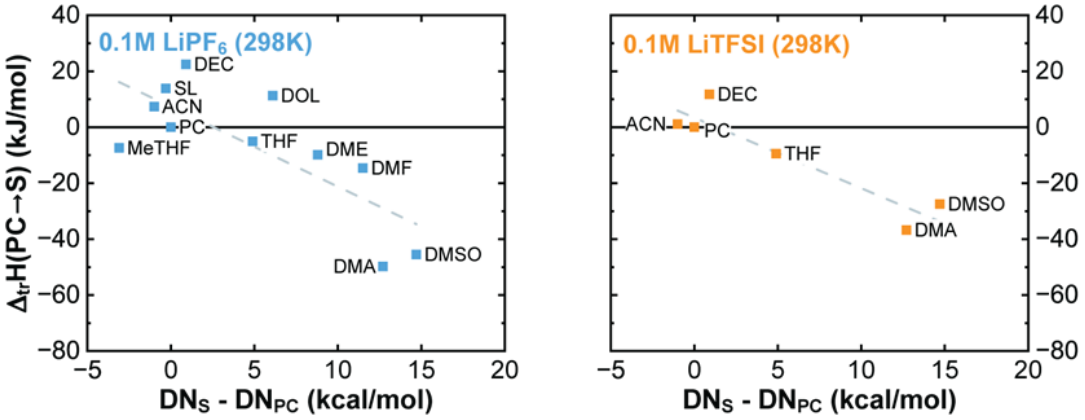

Figure III.3: ***Enthalpies of transfer of $LiPF_6$ and LiTFSI from PC to several aprotic solvents.*** *The enthalpies of transfer are plotted vs. difference in donor number between the solvents. The dashed line highlights a general trend that as the $DN_S - DN_{PC}$ become more positive (i.e. transfer into a stronger lewis acid) the enthalpy of transfer becomes more exothermic.*

electrolyte, and thus are quantitative measurement to establish preferential solvation tendencies. Of course, the entropy of transfer also plays an important role in determining preferential solvation tendencies but is outside the scope of this study. PC was chosen as the reference solvent because it approximates 'infinite' dilution at 0.1 M, providing a well-defined reference state of the ions.

The $\Delta_{\mathrm{tr}}\mathrm{H}$ for $LiPF_6$ and LiTFSI are plotted vs the difference in DN between the transfer solvent and PC in Figure III.3. For both salts we show that at 0.1 M the salts are more enthalpically stable in DMA, DMSO, and THF (and MeTHF, DME, DMF for $LiPF_6$) than in PC, and less enthalpically stable in ACN and DEC (and

SL and DOL for $LiPF_6$). The calculated $\Delta_{tr}H$ of LiTFSI and $LiPF_6$ are compared with other Li salt $\Delta_{tr}H^{\infty}$ reported in literature in Table III.1. The $\Delta_{tr}H^{\infty}$ are calculated from single-ion enthalpies of transfer summarized in Table I.1. It is evident that $\Delta_{tr}H(\mathrm{LiTFSI/LiPF_6}, \mathrm{PC} \rightarrow \mathrm{DMSO})$ are consistent with the reported $\Delta_{tr}H^{\infty}$ for other Li salts. As has been reported in previous studies, the shape of the anion is an important factor in solvation enthalpies,[74] as is seen by the significantly less exothermic $\Delta_{tr}H$ for the linear anions Otf (CF_3SO_3) and TFSI compared to the spherical anions. On the contrary, $\Delta_{tr}H(\mathrm{LiTFSI/LiPF_6}, \mathrm{PC} \rightarrow \mathrm{ACN})$ are endothermic at 0.1 M, whereas for other lithium salts $\Delta_{tr}H^{\infty}$ is exothermic. This difference could be due to significant ion pairing in ACN at 0.1 M, and is a potentially interesting topic of a future study because relative enthalpic stability of these solutions appears to change drastically with salt concentration. This is especially relevant for LMB electrolytes which have seen a trend toward high concentration electrolytes (> 1 M). Further comparison for other solvents is not discussed due to sparsity of data.

Overall, this study of enthalpies of solution and enthalpies of transfer for $LiPF_6$ and LiTFSI is timely for the development of LMB electrolytes and begins to elucidate solvation tendencies in a range of polar aprotic solvents. We show the relevance of solvent donicity on the solvation strength of battery-relevant salts $LiPF_6$ and LiTFSI, and put the data into context with other common Li salts. Further investigation is needed to determine the solution Gibbs free energies and entropies of these salts to fully define the solvation thermodynamics, and studies on the concentration dependence should be conducted for more direct application to battery electrolytes.

Table III.1: ***Enthalpies of transfer of select lithium salts from PC to another aprotic solvent, $\Delta_{tr}H(salt, PC \rightarrow S)$, at 25°C.*** *The enthalpies of transfer at 'infinite' dilution, $\Delta_{tr}H^{\infty}$, are from Y. Marcus, "Ions in Solution and Their Solvation."[44] $\Delta_{tr}H(0.1\ M)$ are calculated from this work.*

	$\Delta_{tr}H(salt, PC \rightarrow S)$ (kJ/mol)									
Solvent (S) =	**ACN**	**DMF**	**DMA**	**DMSO**	**SL**	**THF**	**DEC**	**DOL**	**DME**	**MeTHF**
$\Delta_{tr}H^{\infty}$										
$LiClO_4$	-16.1	-35.3		-33.5						
$LiCF_3SO_3$	-15.0			-28.5						
LiF		-22.5								
LiCl	-23.6	-33.0		-36.8	10.0					
LiBr	-23.4	-37.9		-41.1	7.0					
$LiNO_3$	-13.0			-31.1						
$\Delta_{tr}H(0.1\ M)$										
LiTFSI	1.1		-36.8	-27.4		-9.5	11.8			
$LiPF_6$	7.4	-14.6	-49.8	-45.5	13.8	-5.0	22.5	11.3	-9.9	-7.4

III.2. Calorimetric Titration

III.2.1. The Solvent Displacement Titration

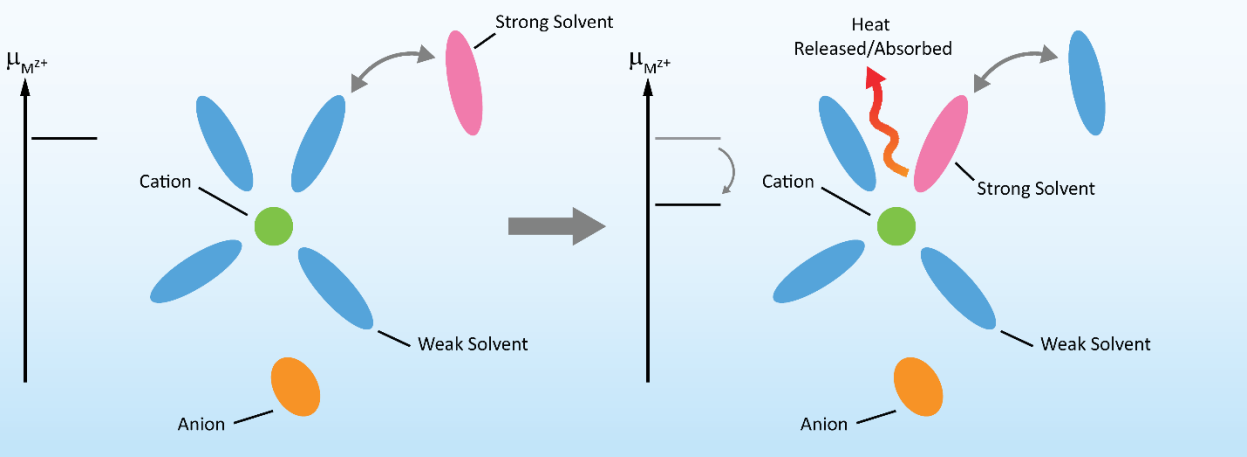

Figure III.4: Solvent displacement scheme utilized for calorimetric and potentiometric titrations. Salt is fully dissociated in a weak solvent, forming solvent separated ion pairs. Introduction of a strong solvent causes the exchange of a weak solvent in the coordination shell for a strong solvent. This process releases/absorbs heat and lowers the chemical potential of the cation to a more favorable state.

The second objective of this work is to measure the enthalpy, Gibbs free energy, and entropy upon coordination of a solvent molecule to Li^+ in a condensed phase. To do so, we must isolate Li^+ from the anion in a liquid state. This requires that the salt be dissolved in an initial solvent at low concentration such that Li^+ exists with a coordination sphere made up of only the chosen initial solvent. In this state, however, we are unable to probe the thermodynamics of coordination because the system is in equilibrium. By introducing a stronger solvent to the initial electrolyte, the coordination shell undergoes a change in its thermodynamic equilibrium state. Heat will be released or absorbed and the chemical potential of Li^+ will change as the energy of the coordination sphere complex changes. These energetic changes can be measured via calorimetric and potentiometric methods as will be discussed below. Figure III.4 illustrates this solvent displacement scheme. In the initial state, the cation and anion exist in solvent-separated (SSIP) or fully-separated (SIP) ion pairs such that only the weak solvent is in the coordination shell. Upon introduction of the strong solvent, weak solvent molecules are dislodged from

the coordination shell and replaced by the strong solvent. In this scheme, the anion should never enter the primary coordination sphere.

Our microcalorimeter (μRC) is a power compensation calorimeter with a sample and reference chamber and auto titration capabilities (Figure III.5a). Both the sample and reference vials are initially filled with the weak electrolyte, and the titration syringe contains the strong solvent which will drive the displacement reaction in the coordination shell of Li^+. As an exemplar case, we chose 0.1 M $LiPF_6$ / ACN as the weak electrolyte, and DMSO as the strong, displacing solvent (Figure III.5b). $LiPF_6$ was chosen for its highly dissociating ability to ensure that there are little to no contact ion pairs even in the weak solvent, ACN. ACN was chosen as the weak solvent particularly for its low donor number in comparison to the strong solvent, DMSO. This means that DMSO is a stronger Lewis base and should preferentially coordinate with Li^+ over ACN. Additionally, ACN has a relatively high dielectric constant compared to other weak solvent choices, which should further minimize ion pairing. Lastly, ACN and DMSO have Raman-active vibrational modes that are mostly non-overlapping and easy to deconvolute, which is necessary for spectroscopic confirmation of solvent displacement. Ideally, we would use lower concentrations of Li around 10^{-3} M to achieve ideal "infinite dilution" behavior, however the sample volume and resolution of our μRC limits how dilute we can make the electrolyte while still generating sufficient heat changes to measure. We found 0.1 M to enable near full dissociation of $LiPF_6$ while also generating a measurable amount of heat during solvent displacement.

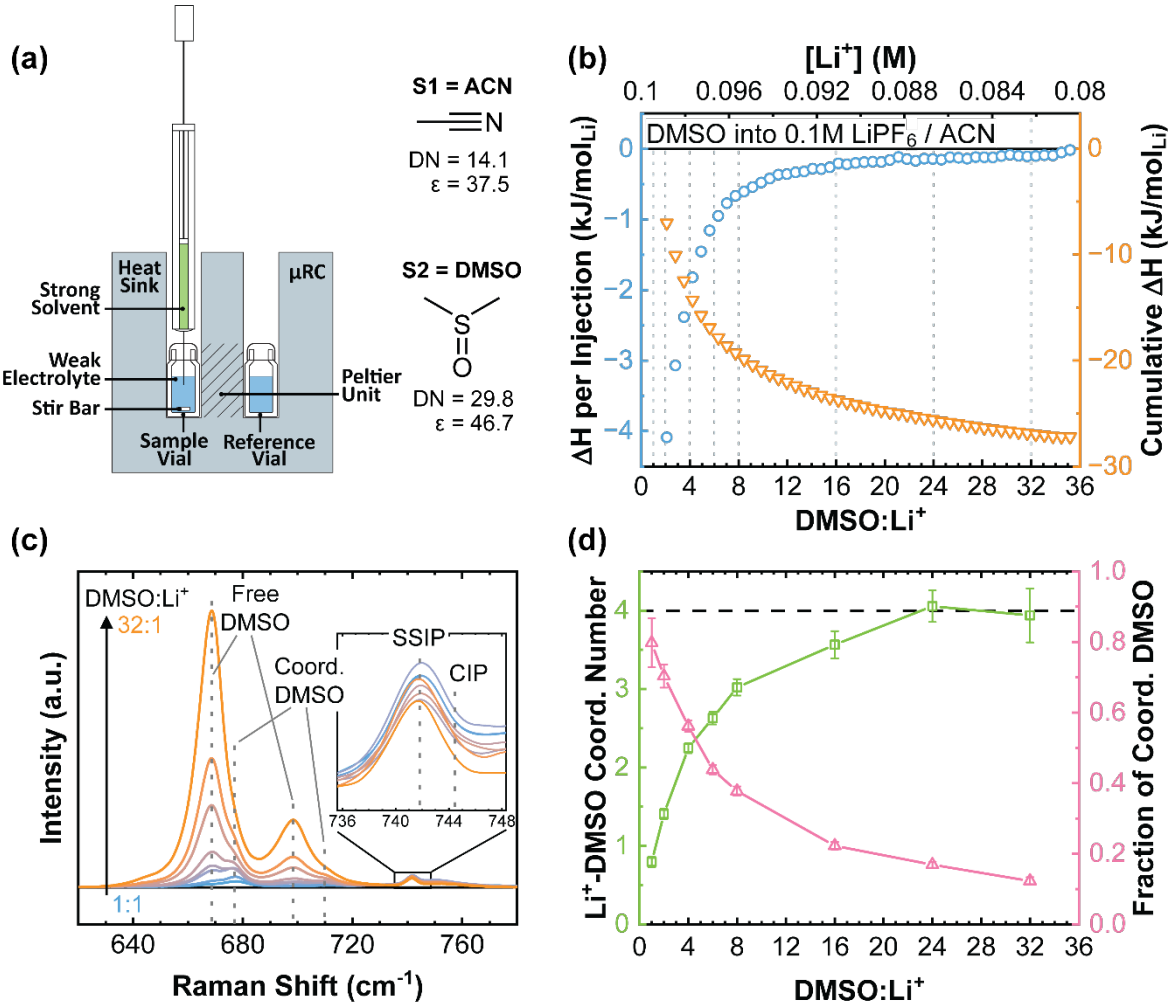

Figure III.5: ***Calorimetric titration method for an exemplar solvent displacement experiment with DMSO as the strong solvent and 0.1 M $LiPF_6$ / ACN as the weak electrolyte. Solvent displacement supported by Raman spectroscopy. (a)*** *Micro Reaction Calorimeter (μRC) setup measures reaction heats. Weak solvent (S1) and strong solvent (S2) chemical structures, donor numbers (DN) in kcal/mol, and dielectric constants (ε).* ***(b)*** *Measured enthalpy change per injection and cumulative enthalpy change vs the ratio of DMSO:Li^+. Measurement is corrected for solvent mixing. Dashed lines indicate mole ratios where Raman samples were taken.* ***(c)*** *Raman spectra of the electrolyte at select DMSO:Li^+ ratios throughout the titration. Vibration modes related to free and coordinated DMSO are labeled, and an enlarged view of the PF_6^- coordination-sensitive vibration modes are shown with labels for solvent-separated ion pairs (SSIP) and contact ion pairs (CIP).* ***(d)*** *Average coordination number of DMSO to Li^+ and the fraction of all DMSO in a coordinated state from deconvolution and integration of data in (c).*

Upon injecting DMSO into the $LiPF_6$ / ACN electrolyte, there are several interactions which may be detected by the μRC: solvent-cation, cation-anion, solvent-solvent, and solvent-anion. Here, we want to isolate just the solvent-cation displacement interaction. Cation-anion interactions are assumed to be negligible since the ions begin and remain in a solvent-separated or fully-solvated state. Because of this, heats associated with the dilution of the salt are also neglected. Solvent-solvent interactions, however, cannot be neglected. They are corrected for by performing a titration of DMSO into neat ACN, and subtracting the resulting mixing heat per injection from the solvent displacement experiment:

$$\mathrm{Q_{corr}} = \mathrm{Q_{meas}} - \mathrm{Q_{mixing}(ACN + DMSO)}$$

Lastly, solvent-anion interactions are thought to be small for the fluorinated PF_6^- anion, however, further investigation of the anion influence will be conducted in the next section.

The resulting corrected ITC isotherm at 25°C for the titration of 50x5 μL injections of DMSO into 1 mL of 0.1 M $LiPF_6$ / ACN is shown in Figure III.5b. This isotherm—which has a decay-like shape—is typical of low affinity reactions.[75, 76] This is because upon the initial injection, most, but not all, of the DMSO displaces ACN and enters the coordination shell of Li^+. This is an exothermic reaction which releases heat proportional to the amount of solvent displacement occurring. In the following injection, some of the ACN is already displaced, and there is less of a driving force for solvent displacement. The measured heat for this the second injection is thus less than the first injection. This continues until all the Li^+ primary coordination spheres become nearly fully saturated with DMSO, and the enthalpy change measured per injection approaches zero.

To confirm that solvent displacement was occurring as expected and that our interpretation of the ITC isotherm was accurate, we used Raman spectroscopy to probe changes in the coordination shell of Li^+ at several points throughout the titration. Figure III.5c shows the Raman spectra of the electrolyte at

solvent and anion vibration modes which are sensitive to Li^+ coordination. The vibrational mode at ~742 cm^{-1} is the P-F stretching mode of PF_6^- in an uncoordinated state. The vibrational mode associated with contact ion paired (CIP) PF_6^- has been previously assigned to ~744.5 cm^{-1}.[77] This mode showed little to no activity throughout the entire titration, indicating that Li^+ is in a fully dissociated state (SSIP/SIP) and our assumption that cation-anion interactions are negligible is valid. The vibrational modes located at 668 cm^{-1} and 698 cm^{-1} correspond to C-S-C symmetric and antisymmetric stretching modes of neat DMSO respectively. The slightly blue-shifted modes at 677 cm^{-1} and 710 cm^{-1} correspond to the C-S-C stretching modes for Li^+-coordinated DMSO. These modes are assumed to have the same intensity coefficients such that the ratio of peak areas of the free vs coordinated DMSO peaks is equal to the ratio of free vs coordinated DMSO concentration.[78] At a DMSO:Li^+ ratio of 1:1, about 80% of the DMSO is in a coordinated state (Figure III.5d). This confirms our interpretation of the ITC isotherm that most, but not all, of the DMSO undergoes solvent displacement in the initial injections. As more DMSO is added, the free DMSO peaks increase at a faster rate, and the fraction of coordinated DMSO decreases. The coordination number (CN) of DMSO to Li^+ increases until the coordination sphere is saturated with about 4 DMSO. A CN of 4 is a common result in Li literature.[33, 78] Note that the increase in CN follows a very similar behavior to the cumulative change in enthalpy measured via ITC, and both identify a fully saturated coordination shell between 16-24 DMSO:Li^+, further confirming that the solvent displacement is the major source of the heat measured.

III.2.1. The Effect of the Anion on Calorimetric Titrations

To further investigate the influence the anion has on the heats measured during our solvent displacement titrations, we performed a series of solvent injections to isolate single ion contributions to the total displacement heat. These experiments were performed by preparing 1 mL of a weak PC electrolyte with a salt concentration of 0.1 M, and then injecting 250 µL of DMSO in a single injection.

Similar to the solvent displacement titration, the measured heat is corrected for the heat of mixing by performing an injection of DMSO into neat PC. The corrected injection enthalpy, $\Delta_{\mathrm{inj}}\mathrm{H}(\mathrm{salt}, 0.1\ \mathrm{M/PC} \rightarrow 0.08\ \mathrm{M}\ /\ \mathrm{PC{:}\,DMSO}\ (4{:}\,1\ \mathrm{vol}))$, is thus the cumulative heat that would be measured from a whole solvent displacement titration experiment with PC and DMSO as the weak and strong solvents, respectively. Here, we are using PC, instead of ACN, as the weak solvent because further reported experiments use PC. This choice is discussed more later and should not affect the following discussion.

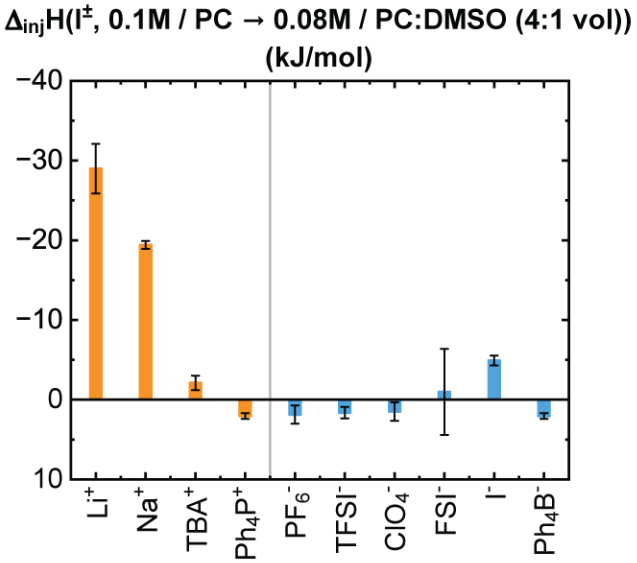

Figure III.6: ***Single ion ($I^{\pm}$) enthalpies of injection of DMSO into 0.1 M PC electrolytes at 25°C.***

To isolate the single-ion enthalpies of injection, we used the TPTB assumption, which assumes that two opposite ions of spherical shape, equal size, and non-solvent-interacting peripheral groups should both have equal effect on their surrounding coordination spheres. This assumption is typically used to obtain enthalpies of transfer of an ion from one solvent to another at 'infinite' dilution, $\Delta_{\mathrm{tr}}\mathrm{H}^{\infty}(\mathrm{I}^{\pm}, \mathrm{R} \rightarrow \mathrm{S})$. Here, we extend the TPTB assumption to apply to our enthalpies of injection:

$$\Delta_{\mathrm{inj}}\mathrm{H}(\mathrm{Ph_4P^+}) = \Delta_{\mathrm{inj}}\mathrm{H}(\mathrm{Ph_4B^-})$$

Due to solubility issues in PC, we were unable directly use the $\mathrm{Ph_4PPh_4B}$ salt. Instead, to obtain $\Delta_{\mathrm{inj}}\mathrm{H}(\mathrm{Ph_4P^+})$ and $\Delta_{\mathrm{inj}}\mathrm{H}(\mathrm{Ph_4B^-})$, we performed a series of single injection measurements with $\mathrm{Ph_4PI}$, $\mathrm{NaPh_4B}$, and NaI, and used the following relationship to calculate single ion contributions:

$$\Delta_{\mathrm{inj}}\mathrm{H}(\mathrm{Ph_4P^+}) = \Delta_{\mathrm{inj}}\mathrm{H}(\mathrm{Ph_4B^-}) = \frac{1}{2}\left(\Delta_{\mathrm{inj}}\mathrm{H}(\mathrm{Ph_4PI}) + \Delta_{\mathrm{inj}}\mathrm{H}(\mathrm{NaPh_4B}) - \Delta_{\mathrm{inj}}\mathrm{H}(\mathrm{NaI})\right)$$

The single ion enthalpies of injection are shown in Figure III.6 (and given in Table A.2). All full salt enthalpies of injection, used to calculate these values, are given in Table A.1. $\Delta_{\mathrm{inj}}\mathrm{H}(\mathrm{Ph_4P^+})$ and $\Delta_{\mathrm{inj}}\mathrm{H}(\mathrm{Ph_4B^-})$ are found to be endothermic and have a magnitude 2.1 kJ/mol. This is close to the reported standard molar enthalpy of transfer of these ions from PC to DMSO ($\Delta_{\mathrm{tr}}\mathrm{H}^{\infty}(\mathrm{Ph_4P^+}, \mathrm{PC} \rightarrow \mathrm{DMSO}) = \Delta_{\mathrm{tr}}\mathrm{H}^{\infty}(\mathrm{Ph_4B^-}, \mathrm{PC} \rightarrow \mathrm{DMSO}) = 2.0\ \mathrm{kJ/mol}$).[44] Our values are expected to be similar, but not equivalent to, standard reported values due to deviation from 'infinite' dilution, mixture of solvents, and dilution during injection; their near equivalence here is coincidental. The closeness of the values, however, supports the validity of applying the TPTB assumption in this work.

For solvent displacement of PC by DMSO in Li salts, the largest contribution to enthalpy change is the exothermic solvent displacement around Li^+ (-29.0 kJ/mol). This is also in good agreement with the standard molar enthalpy of transfer of Li^+ from PC to DMSO (-30.6 kJ/mol), which is consistent with the notion that DMSO preferentially solvates Li^+ and has displaced nearly all PC in the primary coordination sphere by the end of the titration. Critically, we also observe that the PF_6^-, $TFSI^-$, and ClO_4^- (and possibly FSI^-) anions have contributions which are an order of magnitude smaller than that of Li^+. The iodide ion has a larger magnitude contribution likely due to the higher charge density of the monoatomic ion. This confirms our previous assumption that heats measured during ITC are dominated by the solvent displacement around Li^+ when using charge-delocalized anions like PF_6^-. However, it is important to treat

this assumption with caution because the effect of the anion can change be heavily influenced by specific chemical interactions with certain solvents.

III.3. Potentiometric Titration

In principle, the ITC method contains all the information necessary to measure the ΔH, ΔG and ultimately ΔS in a single measurement. The ITC curve shape is dependent on the ΔG of the reactions occurring in the cell, and the amplitude of the curve is dependent on the ΔH of the reactions. In biological and pharmaceutical literature, ITC is frequently used to measure the ΔH, ΔG, and ΔS of ligand binding processes by fitting the ITC curve to a mathematical model. However, most biological ligand binding processes have a much higher affinity than solvent replacement around Li^+. The higher affinity results in a sigmoidal curve which tends to be easier to fit to a binding model. When the curve loses its sigmoidal shape, as seen in our solvent displacement measurements, the ΔH and ΔG in the model become correlated, making it difficult to achieve a confident fit. To resolve this challenge, we needed an independent dataset which can help converge on more accurate values for ΔG of solvent replacement.

Using an electrochemical cell, it is possible to measure the ΔG of a reversible electrochemical reaction with the relationship: $\Delta G = -zFE$, where z is the charge transferred, F is the Faraday constant, and E is the electromotive force (emf) of the cell. S. C. Kim, et al. recently developed a cell with symmetric Li electrodes and asymmetric electrolytes and showed that the cell open circuit potential is related to the $\Delta_{tr}G_{Li^+}$ from a reference electrolyte to a test electrolyte.[20] Our cell, depicted in Figure III.7a, follows the same idea except that in our test electrolyte, we perform a titration similar to ITC. The cell is also represented as follows:

Li	0.1M LiTFSI S1 (reference electrolyte)	1M LiTFSI DOL:DME (salt bridge)	0.1M LiTFSI S1 + S2 (test electrolyte)	Li

where S1 is the weak solvent, and S2 is the strong solvent.

The asymmetric electrolytes in our setup are joined by a salt bridge. Glass frits separate the salt bridge from the reference and test electrolytes to allow for ion transfer while minimizing mixing of the electrolytes. The high concentration of the salt bridge compared to the reference and test electrolytes, along with approximately equal transference numbers of Li^+ and $TFSI^-$, should minimize the liquid junction potentials at the liquid/liquid interfaces.[79] The salt bridge setup was compared vs. $Me_{10}Fc$ redox potential and an Ag/Ag^+ ionic liquid reference electrode. All three setups measured changes in open circuit potential within 5 mV of each other over the course of a titration (Figure A.3), suggesting that the liquid junction potential remains small and nearly constant.

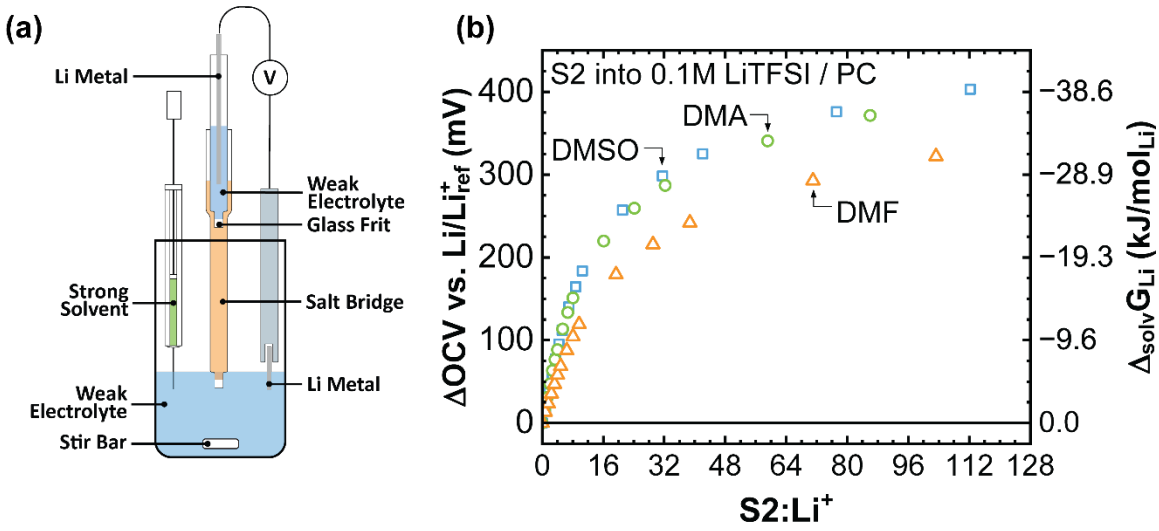

Figure III.7: ***Potentiometric titration method for a few exemplar solvent displacement experiments with DMF, DMSO, and DMA as strong solvents and 0.1 M LiTFSI / PC as the weak electrolyte. (a)*** *Potentiometric titration setup consists of symmetric Li electrodes initially in identical weak electrolytes (blue). The half cells are ionically connected via a salt bridge (orange). The strong solvent (green) is injected in small amounts. The open circuit potential (OCV) of the cell is related to ΔG_{Li^+}.* ***(b)*** *Measured change in OCV vs. the ratio of S2:Li^+. ΔG_{Li^+} is negative, signifying a spontaneous solvent displacement reaction and lower Li^+ chemical potential.*

Although it would be ideal to perform the potentiometric titration (PT) with the same exemplary electrolyte as before (DMSO into 0.1 M $LiPF_6$ / ACN), compatibility issues with Li metal and the salt bridge prohibits the use of PF_6^- and ACN in this setup. Thus, we tested the system using the $TFSI^-$ anion and PC as the weak solvent. Based on the enthalpy of solution experiments, 0.1 M LiTFSI in PC approximates an 'infinitely' dilute solution, and TFSI appears to have similar behavior to PF_6^- in terms of solvent interaction. The open circuit potential at 25 °C was measured after each injection of the strong solvent and the resulting PT curves are shown in Figure III.7b. Note that this data is cumulative whereas ITC data is reported on per injection basis. Also note that by virtue of using an electrochemical cell, we are measuring a difference in Li^+ chemical potentials only, therefore anion-solvent interactions, which introduce an unwanted error to our ITC experiments, should not affect PT results.

The negative Gibbs free energy changes in Figure III.7b signifies that solvent displacement is happening spontaneously and lowering the Li^+ chemical potential. Injection of DMSO induces the largest negative change in Gibbs free energy of the Li coordination complex, followed closely by DMA and then DMF. This is order is slightly different than what we expected from solution enthalpy measurements, where injection of DMA appears to produce larger changes in enthalpy than DMSO, indicating that entropic changes during solvent displacement are significant. To gain further insight and quantify the thermodynamics of the solvent displacement, we developed a mathematical model to describe the reactions occurring during the titration and fit the model to the data.

III.4. Binding Model

The model is adapted from the well-studied binding polynomial, which has been used previously to fit biological ITC data.[70, 71] The binding polynomial is a partition function used to represent the composition of a solution with the stability constants (β_i) of all possible complexes. In conjunction with mass balance equations, it can be used to solve for the concentrations of each possible complex. To define the possible complexes in our electrolyte, we made several assumptions:

1. The cation has N binding sites which are always occupied. N is assumed to be constant for a given cation.
2. Solvents have a single binding site, which can only bind to a cation binding site (i.e. no solvent-solvent interactions)
3. Anions have no binding sites (i.e. no ion pairing, no aggregation, and no solvent-anion interactions)

For Li^+, the total coordination number is typically 4 for most solvents, therefore Li^+ can be said to have N=4 binding sites. We also confirmed that N=4 produces the best fit to the experimental data compared to N=3 and N=5 (Figure A.4). Following the above assumptions, the possible complexes that can form with Li^+ are illustrated in Figure III.8a. A general equation for the stepwise solvent displacement is given below.

$$\mathrm{M^+(S1)_{N-i+1}(S2)_{i-1} + (S2) \rightleftharpoons M^+(S1)_{N-i}\,(S2)_i + (S1)}$$

where $\mathrm{M^+}$ is the metal cation, $\mathrm{S1}$ is the weak solvent, and $\mathrm{S2}$ is the strong solvent, and $\mathrm{i} = 1,2,\ldots,\mathrm{N}$. The notation $\mathrm{M^+(S1)}_p\mathrm{(S2)}_q$ denotes a cation coordination complex with p weak solvent molecules, and q strong solvent molecules in the primary coordination sphere. Using the isothermal-isobaric ensemble,

each stepwise solvent displacement has an associated change in enthalpy (Δh_i) and a thermodynamic equilibrium constant (K_i).

$$K_i = \frac{\{M^+(S1)_{N-i}(S2)_i\}\{S1\}}{\{M^+(S1)_{N-i+1}(S2)_{i-1}\}\{S2\}}$$

where {Y} is the activity of species Y.

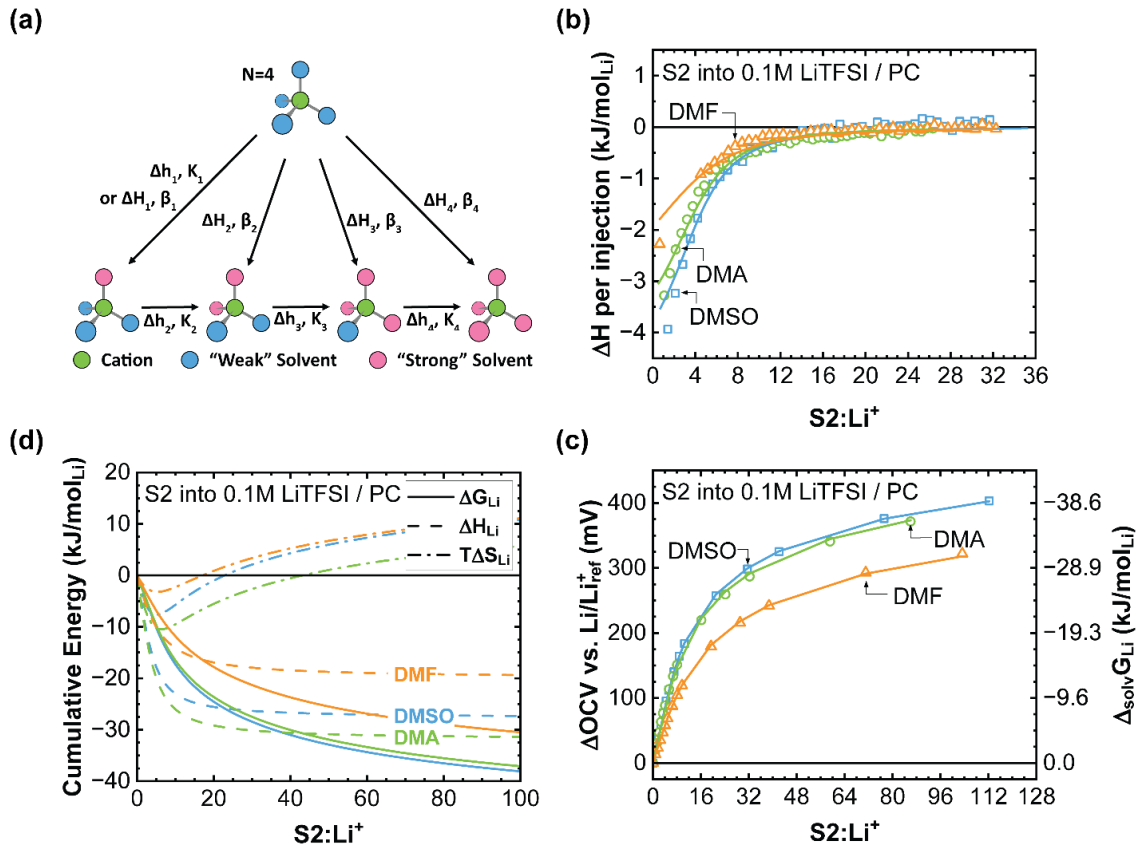

Figure III.8: ***Binding model scheme and exemplar data fitting. (a)*** *Schematic of the possible cation coordination sphere states. N=4 binding sites were chosen for Li^+. The stepwise enthalpies and equilibrium constants are defined as Δh_i and K_i, respectively. The cumulative enthalpies and stability constant) are defined as ΔH_i and β_i, respectively.* ***(b)*** *Enthalpy change per injection vs. the ratio of S2:Li^+ measured via calorimetric titrations. The best model fits are shown with solid lines.* ***(c)*** *Cumulative OCV change vs. the ratio of S2:Li^+ measured via potentiometric titrations. The best model fits are shown with solid lines.* ***(d)*** *The cumulative Gibbs free energy, enthalpy, and entropic energy calculated and extrapolated using the parameters from the best fits.*

Similarly, we can also define a cumulative solvent displacement reaction with an associated cumulative change in enthalpy (ΔH_i) and cumulative equilibrium constant, also known as a stability constant (β_i).

$$M^+(S1)_N + i(S2) \rightleftharpoons M^+(S1)_{N-i}(S2)_i + i(S1)$$

$$\beta_i = \frac{\{M^+(S1)_{N-i}(S2)_i\}\{S1\}^i}{\{M^+(S1)_N\}\{S2\}^i} \qquad \text{where } \Delta G_i = RT\ln(\beta_i)$$

The stepwise and cumulative thermochemistry are related as follows:

$$\Delta H_i = \sum_{j=1}^{i} \Delta h_j \qquad\qquad \beta_i = \prod_{j=1}^{i} K_j$$

The binding polynomial can then be derived by performing a mass balance of the cations in solution and plugging in stability constants. The full derivation with necessary assumptions is detailed in Appendix A1. The resulting equation for the binding polynomial, Z, is

$$Z = \frac{X_{M^+,tot}}{X_{M^+(S1)_N}} = \sum_{i=0}^{N} \beta_i \left(\frac{\{S2\}}{\{S1\}}\right)^i$$

Where X_Y is the mole fraction of species Y. Then, the mole fraction of each complex can be calculated with

$$X_{M^+(S1)_{N-i}(S2)_i} = X_{M^+,tot} \frac{\beta_i \left(\frac{\{S2\}}{\{S1\}}\right)^i}{Z}$$

Note that we still have the activities of uncoordinated S1 and S2 in the equation. These activities are not known. For the purposes of this work, we will assume the solvents follow ideal Rault's law. It states that in an ideal mixture of solvents at equilibrium, the intermolecular forces between the two solvents are identical such that

$$\{S1\} = \frac{P_{S1}}{P_{S1}^0} = X_{S1} \text{ and } \{S2\} = \frac{P_{S2}}{P_{S2}^0} = X_{S2},$$

where P_{S1} and P_{S2} are the partial pressures of S1 and S2 in the headspace of the mixture, P_{S1}^0 and P_{S2}^0 are the vapor pressures of the pure solvents, and X_{S1} and X_{S2} are the equilibrium mole fractions of uncoordinated S1 and S2. These mole fractions are solved for with two additional mass balance equations detailed in Appendix A1. The ideal Rault's law assumption is most likely not valid towards the end of the injections in ITC and PT, as the mole fractions of S1 and S2 deviate significantly from 1 and 0 respectively. The activities of each solvent could be measured throughout the titration via the partial pressure of each gas in the sample headspace to improve the accuracy of the model, however the ideal Rault's law assumption appears to be sufficient to achieve good fitting with the data and thus we will use this approximation in this work. With the mole fractions of all complexes, we can calculate the total change in enthalpy from the initial solvated state, $M^+(S1)_N$.

$$\Delta H_{tot} = \sum_{i=1}^{N} \Delta H_i \, X_{M^+(S1)_{N-i}(S2)_i} \, n_{tot} = \sum_{i=1}^{N} \Delta H_i \, X_{M^+,tot} \, n_{tot} \frac{\beta_i \left(\frac{X_{S2}}{X_{S1}}\right)^i}{Z}$$

Where n_{tot} is the total number of moles in the calorimeter cell. ΔH_{tot} must be calculated for each injection as the mole fractions of the cation and solvents change. From this, the ITC data can be simply calculated via

$$\Delta H_{ITC,j} = \Delta H_{tot,j} - \Delta H_{tot,j-1} = f(\beta_i, \Delta H_i, X_{M^+,tot}, X_{S1,tot}, X_{S2,tot}, n_{tot})$$

Where *j* is the injection number. Nonlinear least squares regression can be used to fit the model to the data by optimizing the parameters β_i and ΔH_i. However, as mentioned previously, β_i and ΔH_i become correlated when the ITC curve loses its sigmoidal shape with low affinity reactions.

We can decorrelate the parameters by simultaneously fitting to our potentiometric dataset which is only dependent on β_i. The emf of our electrochemical cell is expected to be:

$$E_{cell} = \frac{RT}{zF}\left(\ln\frac{X_{M^+,tot,test}}{X_{M^+,tot,ref}} - \ln Z_{test} - N\ln\frac{X_{S1,test}}{X_{S1,ref}}\right) = f(\beta_i, X_{M^+,tot}, X_{S1,tot}, X_{S2,tot})$$

Where R is the gas constant and T is the temperature. The full derivation of this expression can be found in Appendix A1. In fitting the model to the Li PT data, where N=4, we found that the four optimized β_i parameters were very sensitive to the initial conditions for the regression and therefore we were still not able to achieve a confident fit to the data.

To simplify the model even further, we chose to define average solvent displacement enthalpies and stability constants:

$$\Delta\mathcal{H} = \frac{1}{N}\Delta H_N \qquad\qquad \mathcal{K} = (\beta_N)^{1/N}$$

Essentially, we are approximating each binding site as identical. Although this is not true in practice, it is close enough to the actual phenomena that the fits to the data are sufficient. The sequential enthalpies of solvent displacement are simply $\Delta h_i = \Delta\mathcal{H}$. And the sequential equilibrium constants are determined by statistical considerations, covered in more detail in Appendix A1. For N = 4, $K_1 = 4\mathcal{K}$, $K_2 = \frac{3}{2}\mathcal{K}$, $K_3 = \frac{2}{3}\mathcal{K}$, and $K_4 = \frac{1}{4}\mathcal{K}$. The average stability constant $\mathcal{K}$ is the same as the K_{PS} discussed in Section I.4.3.

The fits to the ITC and PT data with this simplified two parameter model are shown in Figure III.8b and c, and parameters reported in Table III.2. Even with all the given assumptions, the model fits the PT data very well, within experimental error. This indicates that our $\mathcal{K}$ values are grounded in reasonable assumptions and can be used as accurate quantitative predictors for Li^+ coordination. On the other hand, the fit to the ITC data is good, but not as precise. In all solvent displacement experiments conducted, the model underpredicts the amount of heat generated in the first injections, and in most cases, the model overpredicts the heat generated in the intermediate/latter injections. It is likely the

case that the sequential displacement enthalpies go as $\Delta h_1 > \Delta h_2 > \Delta h_3 > \Delta h_4$ instead of $\Delta h_1 = \Delta h_2 = \Delta h_3 = \Delta h_4$. The discrepancy could also be a result of other interactions that produce non-negligible amounts of heat such as solvent-anion interactions. It appears, however, that the fit is good enough that $\Delta\mathcal{H}$ is a useful average displacement enthalpy and can be used to quantitatively define solvent binding strengths. Preliminary DFT investigation of the Li-PC-DMSO complex energies supports this claim (Figure A.5).

With our fitted model, we are able to predict how the enthalpy and entropy contribute to changes in the free energy of the electrolyte as the titration proceeds. Entropy is calculated from the free energy and enthalpy change via Gibbs fundamental relation: $\Delta G = \Delta H - T\Delta S$. Figure III.8d displays the model projections for free energy, enthalpy and entropy over the course of a simulated titration. In the initial injections, the solvent displacement is driven by the large negative enthalpy, and the negative $T\Delta S$ values indicate that entropy is decreasing. At some point around 5-7 S2:Li^+, $T\Delta S$ begins to increase meaning that solvent displacement becomes entropically favorable once enough of the strong solvent has been injected. For S2:Li^+ around 7-16, the solvent displacement is both entropically and enthalpically favorable. Any additional solvent displacement after that, is mostly entropically driven.

Table III.2: ***Average stability constants ($\mathcal{K}$) and enthalpies of solvent displacement ($\Delta\mathcal{H}$) for Li^+ in some exemplar binary solvent mixtures with PC as the weak solvent.*** *Values obtained by fitting binding model to both ITC and PT curves.*

S1	S2	Salt	Temp (°C)	$\mathcal{K}$	$\Delta\mathcal{H}$ (kJ/mol)
PC	DMF	0.1 M LiTFSI	25	39.0	-4.99
PC	DMA	0.1 M LiTFSI	25	77.3	-7.97
PC	DMSO	0.1 M LiTFSI	25	85.6	-6.93

III.5. Battery Electrolyte Case Study

III.5.1. Li EC:DMC Electrolyte

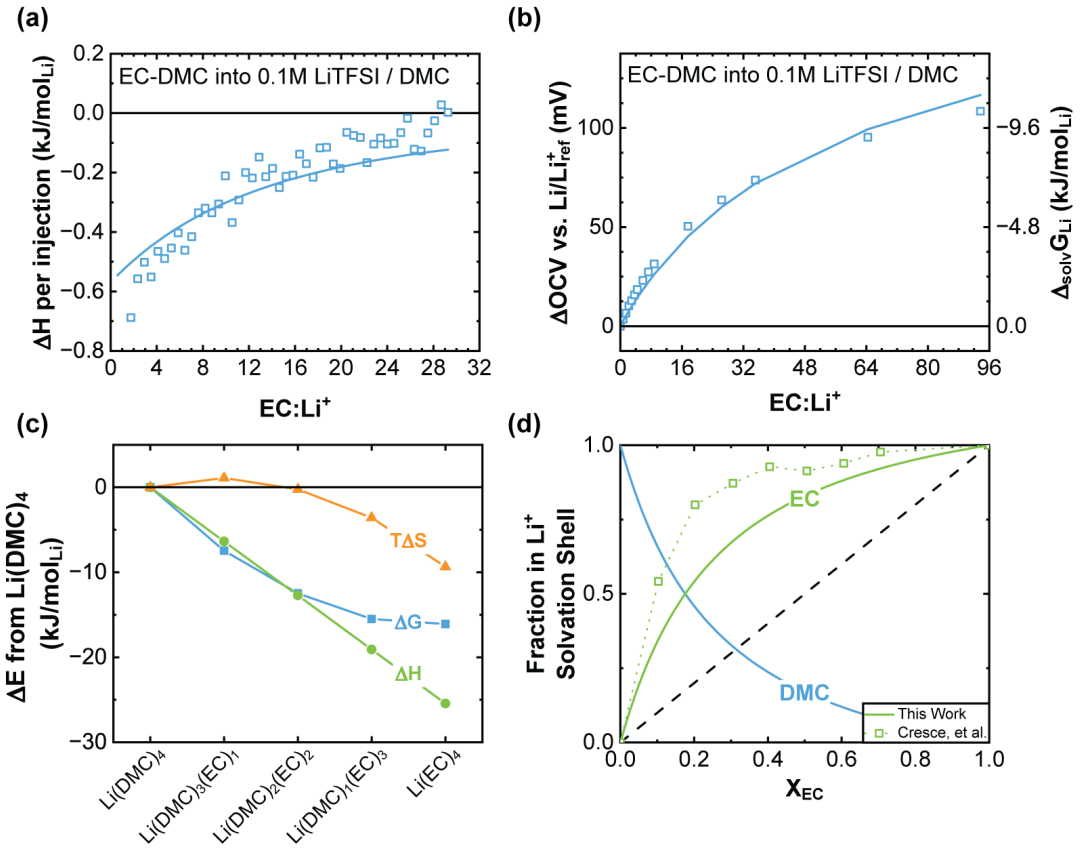

Figure III.9: ***Application of calorimetric and potentiometric titration method to Li electrolyte with EC:DMC binary solvent mixture.*** *(a) Enthalpy per injection vs. the ratio of EC:Li+ measured via calorimetric titrations. The solid line represents the best model fit with parameters* $\mathcal{K} = 5.1$ *and* $\Delta\mathcal{H} = -6.36\ kJ/mol$. *(b) Cumulative OCV change vs. the ratio of EC:Li+ measured via potentiometric titrations. The solid line represents the best model fit. (c) ΔG, ΔH, and ΔS of all possible complexes from the initial state Li(DMC)₄. (d) Coordination number of EC and DMC at different EC:DMC ratios as predicted by the fitted model. The dashed line represents the case where there is no preference between EC and DMC. Open points are reproduced from Cresce, et al.* J. Phys. Chem. C. ***2012***.[3]

To test our method and model's application to a more relevant and well-studied Li battery electrolyte, we performed the method on a Li electrolyte with an EC:DMC solvent blend. The EC:DMC mixture is interesting because it is commonly used in Li-ion batteries with a $LiPF_6$ salt (e.g. 1 M $LiPF_6$ EC:DMC). Both

solvents have low donor numbers (16.4 kcal/mol and 17.2 kcal/mol, for EC and DMC respectively), but EC has a much larger dielectric constant (89.6 vs. 3.1). It has been shown previously through spectroscopic and computational approaches that there is a clear preference for EC in the coordination sphere of Li^+ that is explained in part by the disparity in the dielectric constants.[3, 35, 80, 81] Here, we use our titration experiments to show the same preference, and experimentally quantify the driving forces for this preference.

We conducted calorimetric and potentiometric titrations at 25 °C with EC as the strong solvent and a 0.1 M LiTFSI in DMC weak electrolyte. Since EC is a solid at room temperature, we could not titrate neat EC into the weak electrolyte. Therefore, we used a 3:1 EC:DMC mole ratio mixture as our injectant, which is liquid at room temperature. The responses from the calorimetric and potentiometric titrations are shown in Figure III.9a and b, respectively. Additionally, the best fits achieved by our model are plotted for each (solid line). The fit to the potentiometric data is markedly less good compared to the exemplar solvent displacement experiments with PC as the weak solvent (Figure III.8c). This is probably because of ion pairing that is occurring in the 0.1 M LiTFSI DMC electrolyte before addition of EC, due to the low dielectric constant of DMC. During titration of EC into the electrolyte, the ion pairs will separate and this effect on the thermochemical evolution of the Li^+ solvation environment is not captured by our model. This effect is expected to be small in comparison to solvent displacement, with most error introduced in the first few injections. As such, the effect is largely ignored during this discussion, but the thermochemical parameters of the model should be used with caution.

The relative thermodynamics of the possible Li^+ coordination complexes (as defined by the model), are given in Figure III.9c. The displacement of DMC by EC is driven almost entirely by enthalpic changes in the first two displacement steps. Further displacement is still enthalpically favorable but becomes entropically unfavorable, resulting in a nearly equivalent thermochemical stability of both $Li(DMC)_1(EC)_3$

and $Li(EC)_4$, with only a slight preference for the latter. The enthalpically driven preferential coordination is particularly interesting because the low and similar solvent donor numbers suggest that there would be little difference in the coordination strengths of EC and DMC to Li^+. This preference can be described instead by the large dielectric constant and polarizability of EC, which allows for stronger ion-dipole interactions with Li^+.

Knowing the relative stability of each complex, we can predict the average coordination number (CN) for any mixture of solvents. The predicted CNs of EC and DMC as a function of EC mole fraction, X_{EC}, are plotted in Figure III.9d. It is important to recall that our model assumes ideal Rault's law behavior of the solvents, which is likely not an accurate representation of the solvent activities, especially in the region where there are similar amounts of EC and DMC. Thus, the predicted CNs can only be treated as an approximation of the Li^+ solvation environment. Nonetheless, we observe a preference for EC as indicated by the larger predicted percentage of EC in the coordination shell than DMC for all compositions of the binary solvent mixture. The model CN prediction is compared with results from soft electrospray ionization mass spectroscopy (ESI-MS) studies of the Li^+ coordination sphere of 1.0M $LiPF_6$ EC:DMC electrolytes conducted by Cresce, et al..[3] Our measurements indicate a preference for EC which is less strong than that detected by ESI-MS. Critically, ESI-MS is a destructive technique which detects the Li^+ coordination sphere in the gas phase, and only retains the strongest coordination bonds during the ionization process. Therefore, we suspect that ESI-MS may overpredict coordination numbers of the stronger bonding solvent, EC. If this is the case, the two curves are in even better agreement. It is also important to note the electrolyte conditions in each experiment. In our work, we use 0.1 M LiTFSI when evaluating the preference for EC, and in the ESI-MS study, 1 M $LiPF_6$ was used. This difference in concentration and anion may induce changes in the preference for EC vs DMC which are not considered here. Overall, the complementary calorimetric and potentiometric titrations, along with our

coordination model, agree with the established preference of EC over DMC in the Li^+ first coordination sphere, and provide new quantitative insight into the thermodynamic driving forces behind this preference.

III.5.2. Li EC:PC Electrolyte

As a second application of our method and model, we examined a more contentious Li electrolyte with an EC:PC solvent blend. While an EC:PC solvent blend does not make an effective electrolyte for Li-ion and Li-metal batteries, it has been studied by several groups in an effort to understand why EC can form an effective SEI on graphite, and PC cannot. An older study using Raman spectroscopy came to the conclusion that EC and PC are equally preferred to coordinate to Li^+.[41] And a computational study calculated a slight preference for EC.[82] On the contrary, a more recent study using ESI-MS in conjunction with more modern DFT methods found a significant preference for PC to coordinate to Li^+.[3] We hope to use our method to contribute new data and further develop the understanding of the environment around Li^+ in an EC:PC solvent blend.

We started by performing calorimetric titrations of PC into 0.1 M LiTFSI EC. The titrations were performed at 40 °C because EC is a solid at room temperature. Most of the previously mentioned studies used $LiPF_6$, but due to the incompatibility of PF_6 with our electrochemical cell salt bridge, we had to use TFSI. With either anion, the ions should be near fully dissociated and it should not affect the solvent coordination ability significantly. The ITC response, however, was near zero throughout the titration, indicating that little to no solvent displacement was occurring (Figure III.9a). PT showed similar behavior with only a small change in the emf of the cell due to dilution and changes in solvent activities (Figure III.9b). Note that our temperature control for the potentiometric titrations was poor and the temperature fluctuated between 40-45 °C, thus the potentiometric titrations around 40 °C are subject to larger error. However, even with the larger error, it is quite clear that solvent displacement isn't

occurring to the degree we saw in our previous potentiometric investigations. We also performed PT with reversed weak/strong solvents, EC into 0.1 M LiTFSI PC, and observed similar results, suggesting that neither EC nor PC have a strong preference to coordinate to Li^+. We could not perform the reversed titration with ITC because of EC solidifying in the calorimeter's automated injection assembly.

Attempting to fit to this this data is difficult because the enthalpy and free energy changes are so small. To obtain sufficient displacement reaction heats and emf changes, we proposed using EC and PC as

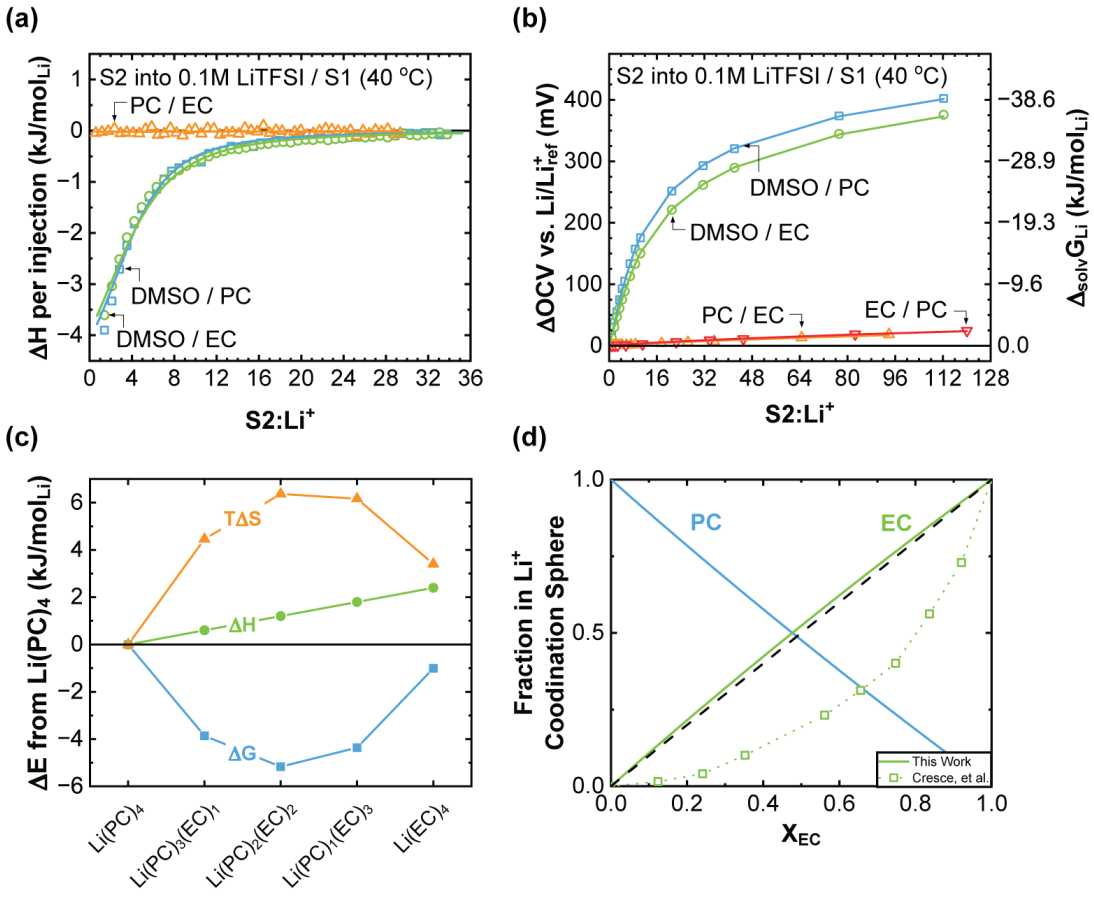

Figure III.10: ***Application of calorimetric and potentiometric titration method to Li electrolyte with EC:PC binary solvent mixture.*** *(a) Enthalpy per injection vs. the ratio of PC:Li+ measured via calorimetric titrations. The solid lines represent the best model fits. (b) Cumulative OCV change vs. the ratio of PC:Li+ measured via potentiometric titrations. The solid lines represent the best model fits. (c) ΔG, ΔH, and ΔS of all possible complexes from the initial state Li(PC)4. (d) Fraction of EC and PC in the primary Li^+ coordination sphere at different EC:PC ratios as predicted by the fitted model. The dashed line represents the case where there is no preference between EC and PC. Open points are reproduced from Cresce, et al.* J. Phys. Chem. C. ***2012***.[3]

weak solvents in two separate experiments. In this way, we could use a much stronger Li^+-coordinating solvent, like DMSO, to indirectly probe the strength of EC and PC coordination to Li^+. The results of these ITC and PT experiments at 40°C are also shown in Figure III.9a and b. Solvent displacement is clearly taking place as expected in these experiments, and the magnitude of the resulting curves are sufficient to obtain confident fits with our simplified two parameter model. The best fits are plotted as solid lines and the best fit parameters are listed in Table III.3. Both EC and PC appear to behave very similarly as weak solvents. If one of them had a higher affinity to coordinate to Li^+, we would expect different ITC and PT responses. Instead, we measure nearly identical ITC curves, and based on the magnitude of the PT curves it appears that PC is a slightly weaker solvent than EC. This is consistent with the previous measurements using EC and PC as the weak and strong solvents.

Next, we used the DMSO solvent displacement thermodynamics to calculate the expected behavior of the EC:PC solvent blend. Since our model assumes each binding site on the cation is identical, we can focus just on the solvent displacement at a single site.

$\mathrm{Li^+_{site}(PC) + DMSO \rightleftharpoons Li^+_{site}(DMSO) + PC}$	$\Delta\mathcal{H}_1$	$\mathcal{K}_1$
$\mathrm{Li^+_{site}(EC) + DMSO \rightleftharpoons Li^+_{site}(DMSO) + EC}$	$\Delta\mathcal{H}_2$	$\mathcal{K}_2$
$\mathrm{Li^+{}_{site}(PC) + EC \rightleftharpoons Li^+_{site}(EC) + PC}$	$\Delta\mathcal{H}_3 = \Delta\mathcal{H}_1 - \Delta\mathcal{H}_2$	$\mathcal{K}_3 = \mathcal{K}_1/\mathcal{K}_2$

Table III.3: ***Average stability constants ($\mathcal{K}$) and enthalpies of solvent displacement ($\Delta\mathcal{H}$) for Li^+ in EC:PC solvent mixture.*** *For S2=DMSO, values obtained by fitting binding model to both ITC and PT curves.*

S1	S2	Salt	Temp (°C)	$\mathcal{K}$	$\Delta\mathcal{H}$ (kJ/mol)
PC	DMSO	0.1 M LiTFSI	40	69.9	-7.86
EC	DMSO	0.1 M LiTFSI	40	63.4	-8.46
PC	EC	0.1 M LiTFSI	40	1.1[a]	0.60[a]

[a] *Calculated from above values as described in the main text.*

Using the above relationship, and still assuming N=4 binding sites, we calculated ΔG, ΔH, and ΔS from an initial state of $Li(PC)_4$. The ΔG were calculated using the same statistical considerations discussed earlier. Figure III.9c illustrates these calculations, and it is evident that there is indeed not a strong Li^+ coordination preference for either EC or PC. The most favorable complex is the one which maximizes entropy, $Li(PC)_2(EC)_2$. There is, however, still a very minor preference for EC as indicated by the -1 kJ/mol_{Li} free energy change from $Li(PC)_4$ to $Li(EC)_4$. Interestingly, although EC is preferred, the positive ΔH trend suggests that it has a smaller binding enthalpy. Thus, the solvent displacement must be driven by entropy in this case. This could perhaps explain why studies using ESI-MS measured a strong preference for PC. The stronger binding enthalpy of PC could mean stronger electrostatic interactions which are able to better withstand the destructive ionization process.

With all the Li^+ complex thermodynamics now quantified, it is possible predict the average CN of each solvent around Li. Figure III.9d shows the calculated CN of EC and PC to Li^+ for all mixtures of EC and PC. The dashed line represents the expected CN of EC if there was no preference for either solvent. The small preference for EC is evident in the slight upward deviation from the dashed line. It is important to note again that the model assumes that the solvent activities follow ideal Rault's Law. As such, this is only an approximation of the CN of EC and PC. Significant deviation from the ideal behavior will surely change the CNs, but it is not expected that the solvent activities will change the behavior enough to create a strong preference for either EC or PC, especially because EC and PC have similar chemical structures.

IV. Conclusions

This thesis explored the direct measurement of thermodynamic driving forces for the solvation of Li^+ in polar aprotic solvents. Solution microcalorimetry was used to measure $\Delta_{sol}H$ and $\Delta_{tr}H$ of two Li-battery relevant salts, $LiPF_6$ and LiTFSI. From the measurements, a weak correlation between the enthalpy of solution and the solvent donicity was established: higher solvent donicity results in stronger cation-solvent interactions which leads to more exothermic $\Delta_{sol}H$. The donicity, however, cannot fully describe the apparent ordering of solvent coordination strengths, which may also be dependent on solvent-anion and solvent-solvent interactions. This data may be useful to Li battery community in the understanding and development of new Li electrolytes.

Both ITC and PT were used to probe the evolution of the Li^+ coordination sphere thermodynamics as weak solvents in the primary coordination sphere are gradually displaced by a stronger solvent. Development and application of a statistical binding model allowed for extraction of average binding constants, $\mathcal{K}$, and average enthalpies, $\Delta\mathcal{H}$, of solvent displacement. Application of the method and model on a set of exemplary electrolytes led to the following quantitative ordering of Li^+ selective solvation vs. PC, a weak solvent: DMSO ($\mathcal{K} = 85.6$), DMA ($\mathcal{K} = 77.3$), DMF ($\mathcal{K} = 39.0$). Interestingly, the ordering of Li^+ coordination enthalpy changes vs. PC was slightly different: DMA ($\Delta\mathcal{H} = -7.97\ \mathrm{kJ/mol}$), DMA ($\Delta\mathcal{H} = -6.93\ \mathrm{kJ/mol}$), DMF ($\Delta\mathcal{H} = -4.99\ \mathrm{kJ/mol}$). This emphasizes the importance of entropic effects in the Li^+ coordination environment. In using this data, it is important to remember there are several assumptions in the model which may contribute to errors in the reported thermochemical parameters. Here, Raman was used to justify assumptions of ion pair dissociation, and carefully designed calorimetry experiments partially justified the assumed non-interaction of solvents and anions. Further work will need to be done to quantify errors from other assumptions.

The preferential solvation tendencies in an EC:DMC Li electrolyte was quantified using our methodology and compared with results from literature, and was found to be in general agreement with the established preference for the cyclic carbonate, EC, to be in the Li^+ first coordination sphere. The magnitude of the preference was found, by our method, to be less great than that found via ESI-MS. In a similar way, the preferential solvation tendencies in an EC:PC Li electrolyte was investigated and compared with conclusions from other workers. With our method, EC was found to be only very slightly preferred over PC, which is in stark contrast to strong preference for PC observed via ESI-MS, but in good agreement with some older Raman and computation studies. However, due to the different experimental conditions across studies, and the assumptions that go into our methods, we cannot yet make a claim on the true nature of the Li^+ coordination spheres in these Li-battery electrolytes. We suspect that ESI-MS may overpredict coordination of solvent with stronger cation interactions, but further investigation is needed.

This thesis has provided a novel viewpoint on the investigation and design of battery electrolytes through a thermodynamic lens. With the data reported here, we can quantitatively predict the coordination environment of Li^+ in any combination of the studied polar aprotic solvents. We are hopeful that this methodology will enable faster and more targeted development of new electrolyte for Li metal batteries and beyond, but there is still work to be done to verify the accuracy of the method. Future work will continue to develop our binding model to incorporate non-ideal solvent mixing, ion pairing, and concentration dependence of both. Further, the method will be applied to the more complex and less understood Ca^{2+} coordination environment, which may have implications for future development of Ca metal batteries. This work provides the foundation to obtain a full thermodynamic picture of the electrolyte coordination environment, which will be used to help elucidate SEI formation pathways and unlock new design principles for any battery chemistry.

References

(1) Liang, Y.; Dong, H.; Aurbach, D.; Yao, Y. Current status and future directions of multivalent metal-ion batteries. *Nature Energy* **2020**, *5* (9), 646-656. DOI: 10.1038/s41560-020-0655-0

(2) Clune, G.; Waghorne, W. E.; Cox, B. G. Solvent coordination and free energies of transfer of cations in dipolar aprotic solvents. *Journal of the Chemical Society, Faraday Transactions 1* **1976**, *72* (0), 1294-1299.

(3) Von Wald Cresce, A.; Borodin, O.; Xu, K. Correlating Li^+ Solvation Sheath Structure with Interphasial Chemistry on Graphite. *The Journal of Physical Chemistry C* **2012**, *116* (50), 26111-26117. DOI: 10.1021/jp303610t

(4) IEA. *Net Zero by 2050*; IEA, Paris, 2021. https://www.iea.org/reports/net-zero-by-2050.

(5) Schmuch, R.; Wagner, R.; Hörpel, G.; Placke, T.; Winter, M. Performance and cost of materials for lithium-based rechargeable automotive batteries. *Nature Energy* **2018**, *3* (4), 267-278. DOI: 10.1038/s41560-018-0107-2

(6) Deng, J.; Bae, C.; Denlinger, A.; Miller, T. Electric Vehicles Batteries: Requirements and Challenges. *Joule* **2020**, *4* (3), 511-515. DOI: 10.1016/j.joule.2020.01.013 (acccessed 2023-07-25T19:57:00).

(7) Xu, W.; Wang, J.; Ding, F.; Chen, X.; Nasybulin, E.; Zhang, Y.; Zhang, J.-G. Lithium metal anodes for rechargeable batteries. *Energy Environ. Sci.* **2014**, *7* (2), 513-537. DOI: 10.1039/c3ee40795k

(8) Liu, B.; Zhang, J.-G.; Xu, W. Advancing Lithium Metal Batteries. *Joule* **2018**, *2* (5), 833-845. DOI: 10.1016/j.joule.2018.03.008

(9) Lin, D.; Liu, Y.; Cui, Y. Reviving the lithium metal anode for high-energy batteries. *Nature Nanotechnology* **2017**, *12* (3), 194-206. DOI: 10.1038/nnano.2017.16

(10) Cao, R.; Mishra, K.; Li, X.; Qian, J.; Engelhard, M. H.; Bowden, M. E.; Han, K. S.; Mueller, K. T.; Henderson, W. A.; Zhang, J.-G. Enabling room temperature sodium metal batteries. *Nano Energy* **2016**, *30*, 825-830. DOI: 10.1016/j.nanoen.2016.09.013

(11) Muldoon, J.; Bucur, C. B.; Gregory, T. Quest for Nonaqueous Multivalent Secondary Batteries: Magnesium and Beyond. *Chemical Reviews* **2014**, *114* (23), 11683-11720. DOI: 10.1021/cr500049y

(12) Eftekhari, A.; Jian, Z.; Ji, X. Potassium Secondary Batteries. *ACS Applied Materials & Interfaces* **2017**, *9* (5), 4404-4419. DOI: 10.1021/acsami.6b07989

(13) Melemed, A. M.; Khurram, A.; Gallant, B. M. Current Understanding of Nonaqueous Electrolytes for Calcium-Based Batteries. *Batteries & Supercaps* **2020**, *3* (7), 570-580. DOI: 10.1002/batt.201900219

(14) Arroyo-De Dompablo, M. E.; Ponrouch, A.; Johansson, P.; Palacín, M. R. Achievements, Challenges, and Prospects of Calcium Batteries. *Chemical Reviews* **2020**, *120* (14), 6331-6357. DOI: 10.1021/acs.chemrev.9b00339

(15) Peled, E.; Menkin, S. Review—SEI: Past, Present and Future. *Journal of The Electrochemical Society* **2017**, *164* (7), A1703-A1719. DOI: 10.1149/2.1441707jes

(16) Cheng, X.-B.; Zhang, R.; Zhao, C.-Z.; Zhang, Q. Toward Safe Lithium Metal Anode in Rechargeable Batteries: A Review. *Chemical Reviews* **2017**, (117), 10403-10473. DOI: 10.1021/acs.chemrev.7b00115.

(17) Tikekar, M. D.; Choudhury, S.; Tu, Z.; Archer, L. A. Design principles for electrolytes and interfaces for stable lithium-metal batteries. *Nature Energy* **2016**, *1* (9), 16114. DOI: 10.1038/nenergy.2016.114

(18) Hobold, G. M.; Lopez, J.; Guo, R.; Minafra, N.; Banerjee, A.; Shirley Meng, Y.; Shao-Horn, Y.; Gallant, B. M. Moving beyond 99.9% Coulombic efficiency for lithium anodes in liquid electrolytes. *Nature Energy* **2021**, *6* (10), 951-960. DOI: 10.1038/s41560-021-00910-w

(19) Xu, K. Electrolytes and Interphases in Li-Ion Batteries and Beyond. *Chemical Reviews* **2014**, *114* (23), 11503-11618. DOI: 10.1021/cr500003w.

(20) Kim, S. C.; Kong, X.; Vilá, R. A.; Huang, W.; Chen, Y.; Boyle, D. T.; Yu, Z.; Wang, H.; Bao, Z.; Qin, J.; et al. Potentiometric Measurement to Probe Solvation Energy and Its Correlation to Lithium Battery

Cyclability. *Journal of the American Chemical Society* **2021**, *143* (27), 10301-10308. DOI: 10.1021/jacs.1c03868
(21) Zhang, X.-Q.; Chen, X.; Hou, L.-P.; Li, B.-Q.; Cheng, X.-B.; Huang, J.-Q.; Zhang, Q. Regulating Anions in the Solvation Sheath of Lithium Ions for Stable Lithium Metal Batteries. *ACS Energy Letters* **2019**, *4* (2), 411-416. DOI: 10.1021/acsenergylett.8b02376
(22) Ren, X.; Gao, P.; Zou, L.; Jiao, S.; Cao, X.; Zhang, X.; Jia, H.; Engelhard, M. H.; Matthews, B. E.; Wu, H.; et al. Role of inner solvation sheath within salt–solvent complexes in tailoring electrode/electrolyte interphases for lithium metal batteries. *Proceedings of the National Academy of Sciences* **2020**, *117* (46), 28603-28613. DOI: 10.1073/pnas.2010852117
(23) Hou, T.; Yang, G.; Rajput, N. N.; Self, J.; Park, S.-W.; Nanda, J.; Persson, K. A. The influence of FEC on the solvation structure and reduction reaction of $LiPF_6$/EC electrolytes and its implications for solid electrolyte interphase formation. *Nano Energy* **2019**, *64*. DOI: 10.1016/j.nanoen.2019.103881.
(24) Gao, X.; Liu, X.; Mariani, A.; Elia, G. A.; Lechner, M.; Streb, C.; Passerini, S. Alkoxy-functionalized ionic liquid electrolytes: understanding ionic coordination of calcium ion speciation for the rational design of calcium electrolytes. *Energy & Environmental Science* **2020**, *13* (8), 2559-2569. DOI: 10.1039/d0ee00831a
(25) Hou, Z.; Zhou, R.; Yao, Y.; Min, Z.; Lu, Z.; Zhu, Y.; Tarascon, J. M.; Zhang, B. Correlation between Electrolyte Chemistry and Solid Electrolyte Interphase for Reversible Ca Metal Anodes. *Angewandte Chemie International Edition* **2022**, *61* (50). DOI: 10.1002/anie.202214796
(26) Cao, L.; Li, D.; Hu, E.; Xu, J.; Deng, T.; Ma, L.; Wang, Y.; Yang, X.-Q.; Wang, C. Solvation Structure Design for Aqueous Zn Metal Batteries. *Journal of the American Chemical Society* **2020**, *142* (51), 21404-21409. DOI: 10.1021/jacs.0c09794
(27) Cheng, H.; Sun, Q.; Li, L.; Zou, Y.; Wang, Y.; Cai, T.; Zhao, F.; Liu, G.; Ma, Z.; Wahyudi, W.; et al. Emerging Era of Electrolyte Solvation Structure and Interfacial Model in Batteries. *ACS Energy Letters* **2022**, *7* (1), 490-513. DOI: 10.1021/acsenergylett.1c02425
(28) Leon, N. J.; Xie, X.; Yang, M.; Driscoll, D. M.; Connell, J. G.; Kim, S.; Seguin, T.; Vaughey, J. T.; Balasubramanian, M.; Persson, K. A.; et al. Room-Temperature Calcium Plating and Stripping Using a Perfluoroalkoxyaluminate Anion Electrolyte. *The Journal of Physical Chemistry C* **2022**, *126* (32), 13579-13584. DOI: 10.1021/acs.jpcc.2c03272
(29) Wang, X.; Toroz, D.; Kim, S.; Clegg, S. L.; Park, G.-S.; Di Tommaso, D. Density functional theory based molecular dynamics study of solution composition effects on the solvation shell of metal ions. *Physical Chemistry Chemical Physics* **2020**, *22* (28), 16301-16313. DOI: 10.1039/d0cp01957g
(30) Bogle, X.; Vazquez, R.; Greenbaum, S.; Cresce, A. V. W.; Xu, K. Understanding Li^+–Solvent Interaction in Nonaqueous Carbonate Electrolytes with ^{17}O NMR. *The Journal of Physical Chemistry Letters* **2013**, *4* (10), 1664-1668. DOI: 10.1021/jz400661k
(31) Suo, L.; Xue, W.; Gobet, M.; Greenbaum, S. G.; Wang, C.; Chen, Y.; Yang, W.; Li, Y.; Li, J. Fluorine-donating electrolytes enable highly reversible 5-V-class Li metal batteries. *Proceedings of the National Academy of Sciences* **2018**, *115* (6), 1156-1161. DOI: 10.1073/pnas.1712895115
(32) Zhao, Y.; Zhou, T.; Ashirov, T.; Kazzi, M. E.; Cancellieri, C.; Jeurgens, L. P. H.; Choi, J. W.; Coskun, A. Fluorinated ether electrolyte with controlled solvation structure for high voltage lithium metal batteries. *Nature Communications* **2022**, *13* (1). DOI: 10.1038/s41467-022-29199-3
(33) Seo, D. M.; Borodin, O.; Han, S.-D.; Boyle, P. D.; Henderson, W. A. Electrolyte Solvation and Ionic Association II. Acetonitrile-Lithium Salt Mixtures: Highly Dissociated Salts. *Journal of The Electrochemical Society* **2012**, *159* (9), A1489-A1500. DOI: 10.1149/2.035209jes
(34) Chapman, N.; Borodin, O.; Yoon, T.; Nguyen, C. C.; Lucht, B. L. Spectroscopic and Density Functional Theory Characterization of Common Lithium Salt Solvates in Carbonate Electrolytes for Lithium Batteries. *The Journal of Physical Chemistry C* **2017**, *121* (4), 2135-2148. DOI: 10.1021/acs.jpcc.6b12234

(35) Seo, D. M.; Reininger, S.; Kutcher, M.; Redmond, K.; Euler, W. B.; Lucht, B. L. Role of Mixed Solvation and Ion Pairing in the Solution Structure of Lithium Ion Battery Electrolytes. *The Journal of Physical Chemistry C* **2015**, *119* (25), 14038-14046. DOI: 10.1021/acs.jpcc.5b03694
(36) Giorgini, M. G.; Futamatagawa, K.; Torii, H.; Musso, M.; Cerini, S. Solvation Structure around the Li^+ Ion in Mixed Cyclic/Linear Carbonate Solutions Unveiled by the Raman Noncoincidence Effect. *The Journal of Physical Chemistry Letters* **2015**, *6* (16), 3296-3302. DOI: 10.1021/acs.jpclett.5b01524
(37) Cao, X.; Jia, H.; Xu, W.; Zhang, J.-G. Review—Localized High-Concentration Electrolytes for Lithium Batteries. *Journal of The Electrochemical Society* **2021**, *168* (1), 010522. DOI: 10.1149/1945-7111/abd60e
(38) Wan, C.; Hu, M. Y.; Borodin, O.; Qian, J.; Qin, Z.; Zhang, J.-G.; Hu, J. Z. Natural abundance ^{17}O, ^{6}Li NMR and molecular modeling studies of the solvation structures of lithium bis(fluorosulfonyl)imide/1,2-dimethoxyethane liquid electrolytes. *Journal of Power Sources* **2016**, *307*, 231-243. DOI: 10.1016/j.jpowsour.2015.12.120
(39) Covington, A. K.; Lilley, T. H.; Newman, K. E.; Porthouse, G. A. Nuclear magnetic resonance studies of preferential solvation. Part 1.—Hydrogen peroxide + water. *Journal of the Chemical Society, Faraday Transactions 1: Physical Chemistry in Condensed Phases* **1973**, *69* (0), 963-972. DOI: 10.1039/F19736900963.
(40) Fukushima, T.; Matsuda, Y.; Hashimoto, H.; Arakawa, R. Studies on Solvation of Lithium Ions in Organic Electrolyte Solutions by Electrospray Ionization-Mass Spectroscopy. *Electrochemical and Solid-State Letters* **2001**, *4* (8), A127. DOI: 10.1149/1.1383428
(41) Hyodo, S.-A.; Okabayashi, K. Raman intensity study of local structure in non-aqueous electrolyte solutions-II. Cation-solvent interaction in mixed solvent systems and selective solvation. *Electrochimica Acta* **1989** *34* (11), 1557-1561. DOI: 10.1016/0013-4686(89)87041-0.
(42) Bhatt, M. D.; Cho, M.; Cho, K. Conduction of Li^+ cations in ethylene carbonate (EC) and propylene carbonate (PC): comparative studies using density functional theory. *Journal of Solid State Electrochemistry* **2012**, *16* (2), 435-441. DOI: 10.1007/s10008-011-1350-7
(43) Davies, C. W. *Ion Association*; Butterworths, **1962**.
(44) Marcus, Y. Ions in Solution and their Solvation. **2015**. DOI: 10.1002/9781118892336
(45) Alexander, R.; Parker, A. J.; Sharp, J. H.; Waghorne, W. E. Solvation of Ions. XVI. Solvent Activity Coefficients of Single Ions. A Recommended Extrathermodynamic Assumption. *Journal of the American Chemical Society* **1972**, *94* (4), 1148-1158. DOI: 10.1021/ja00759a020.
(46) Cox, B. G.; Parker, A. J. Solvation of ions. XVII. Free energies, heats, and entropies of transfer of single ions from protic to dipolar aprotic solvents. *Journal of the American Chemical Society* **1973**, *95* (2), 402-407
(47) Banerjee, D.; Laha, A. K.; Bagchi, S. Preferential solvation in mixed binary solvent. *Journal of the Chemical Society, Faraday Transactions* **1995**, *91* (4), 631. DOI: 10.1039/ft9959100631
(48) Covington, A. K.; Newman, K. E. Thermodynamics of Preferential Solvation of Electrolytes in Binary Solvent Mixtures. In *Advances in Chemistry*, Vol. 155; American Chemical Society, 1976; pp 153-196.
(49) Marcus, Y. Preferential solvation of ions in mixed solvents. Part 4.—Comparison of the Kirkwood–Buff and quasi-lattice quasi-chemical approaches. *Journal of the Chemical Society, Faraday Transactions 1: Physical Chemistry in Condensed Phases* **1989**, *85* (9), 3019. DOI: 10.1039/f19898503019
(50) Marcus, Y. Preferential solvation. Part 3.—Binary solvent mixtures. *Journal of the Chemical Society, Faraday Transactions 1: Physical Chemistry in Condensed Phases* **1989**, *85* (2), 381. DOI: 10.1039/f19898500381
(51) Piekarski, H. Thermochemistry of electrolyte solutions. *Journal of Thermal Analysis and Calorimetry* **2012**, *108* (2), 537-545. DOI: 10.1007/s10973-011-2019-2

(52) Balk, R. W.; Somsen, G. Preferential Solvation and Hydrophobic Hydration of Polyols in Mixtures of Water and N,N-Dimethylformamide. *The Journal of Physical Chemistry* **1985**, *89* (23), 5093-5097. DOI: 10.1021/j100269a041.
(53) Covington, A. D.; Covington, A. K. Nuclear magnetic resonance studies of preferential solvation. Part 5.—Magnesium perchlorate in water + acetone mixtures at 185 K. *Journal of the Chemical Society, Faraday Transactions 1: Physical Chemistry in Condensed Phases* **1975**, *71* (0), 831. DOI: 10.1039/f19757100831
(54) Covington, A. K.; Thain, J. M. Nuclear magnetic resonance studies of preferential solvation. Part 4.—Thermodynamic treatment involving non-statistical distribution of solvated species. *Journal of the Chemical Society, Faraday Transactions 1: Physical Chemistry in Condensed Phases* **1974**, *70* (0), 1879. DOI: 10.1039/f19747001879
(55) Covington, A. K.; Lantzke, I. R.; Thain, J. M. Nuclear magnetic resonance studies of preferential solvation. Part 3.—Thermodynamic treatment involving change of solvation number, and application to dimethyl sulphoxide-containing solvents. *Journal of the Chemical Society, Faraday Transactions 1: Physical Chemistry in Condensed Phases* **1974**, *70* (0), 1869. DOI: 10.1039/f19747001869
(56) Covington, A. K.; Newman, K. E.; Lilley, T. H. Nuclear magnetic resonance studies of preferential solvation. Part 2.—Thermodynamic treatment and application to methanol + water solvents. *Journal of the Chemical Society, Faraday Transactions 1: Physical Chemistry in Condensed Phases* **1973**, *69* (0), 973. DOI: 10.1039/f19736900973
(57) De Valera, E.; Feakins, D.; Waghorne, W. E. Relationship between the enthalpy of transfer of a solute and the thermodynamic mixing functions of mixed solvents. *Journal of the Chemical Society, Faraday Transactions 1: Physical Chemistry in Condensed Phases* **1983**, *79* (5), 1061. DOI: 10.1039/f19837901061
(58) Inerowicz, H.; Kamienska-Piotrowicz, E. Calorimetric study of the solvation of some ions in acetonitrile-dimethylsulfoxide mixtures. *Thermochimica Acta* **1989**, *145*, 219-226. DOI: 10.1016/0040-6031(89)85141-X.
(59) Kamieńska-Piotrowicz, E.; Inerowicz, H. Ionic enthalpies of transfer in acetonitrile–water mixtures. *J. Chem. Soc., Faraday Trans.* **1990**, *86* (20), 3391-3394. DOI: 10.1039/ft9908603391
(60) Bjerrum, J.; Einar, C. Metal Ammine formation in aqueous solution: theory of the reversible step reactions. Copenhagen, **1941**.
(61) Izutsu, K.; Nomura, T.; Nakamura, T.; Kazama, H.; Nakajima, S. The Complexing of the Sodium Ion in Acetonitrile with Other Solvents. Investigation by the Use of a Cation-sensitive Glass Electrode. *Bulletin of the Chemical Society of Japan* **1974**, *47* (7), 1657-1660
(62) Nakamura, T.; Higuchi, H.; Izutsu, K. The Complexing of the Magnesium and Barium Ions in Acetonitrile with Other Solvents. Investigation by the Use of a Polyacrylamide-Tetraethylene Glycol Monododecyl Ether Membrane Ion-Selective Electrode. *Bulletin of the Chemical Society of Japan* **1988**, *61* (3), 1020-1022. DOI: 10.1246/bcsj.61.1020
(63) Nakamura, T. The Complexing of the Thallium(I) Ion with Other Solvents in Acetonitrile. Investigation Using a Cationsensitive Glass Electrode. *Bulletin of the Chemical Society of Japan* **1976**, *49* (5), 1304-1307. DOI: 10.1246/bcsj.49.1304
(64) Nakamura, T. The Complexing of the Lithium Ion in Acetonitrile with Other Solvents. Investigation by the Use of a Cation-sensitive Glass Electrode. *Bulletin of the Chemical Society of Japan* **1975**, *48* (5), 1447-1451. DOI: 10.1246/bcsj.48.1447
(65) Izutsu, K.; Nakamura, T.; Miyoshi, K.; Kurita, K. Potentiometric study of complexation and solvation of lithium ions in some solvents related to lithium batteries. *Electrochimica Acta* **1996**, *41* (16), 2523-2527.

(66) Izutsu, K.; Nakamura, T.; Murayama, T.; Fujinaga, T. The Complexing of the Ammonium Ion in Acetonitrile with Other Solvents. Investigation Using a Cation-sensitive Glass Electrode. *Bulletin of the Chemical Society of Japan* **1978**, *51* (10), 2905-2908. DOI: 10.1246/bcsj.51.2905
(67) Christensen, J. J.; Izatt, R. M.; Hansen, L. D.; Partridge, J. A. Entropy Titration. A Calorimetric Method for the Determination of ΔG, ΔH, and ΔS from a Single Thermometric Titration. *The Journal of Physical Chemistry* **1966**, *70* (6), 2003-2010. DOI: 10.1021/j100878a049
(68) Velazquez-Campoy, A. Geometric features of the Wiseman isotherm in isothermal titration calorimetry. *Journal of Thermal Analysis and Calorimetry* **2015**, *122* (3), 1477-1483. DOI: 10.1007/s10973-015-4775-x
(69) Archer, W. R.; Schulz, M. D. Isothermal titration calorimetry: practical approaches and current applications in soft matter. *Soft Matter* **2020**, *16* (38), 8760-8774. DOI: 10.1039/d0sm01345e
(70) Freyer, M. W.; Lewis, E. A. Isothermal titration calorimetry: experimental design, data analysis, and probing macromolecule/ligand binding and kinetic interactions. In *Methods in Cell Biology*, Vol. 84; **2008**; pp 79-113.
(71) Velazquez-Campoy, A.; Freire, E. Isothermal titration calorimetry to determine association constants for high-affinity ligands. *Nature Protocols* **2006**, *1* (1), 186-191. DOI: 10.1038/nprot.2006.28
(72) Chaban, V. Solvation of the fluorine containing anions and their lithium salts in propylene carbonate and dimethoxyethane. *Journal of Molecular Modeling* **2015**, *21* (7). DOI: 10.1007/s00894-015-2717-y
(73) Ue, M. Mobility and Ionic Association of Lithium and Quaternary Ammonium Salts in Propylene Carbonate and γ-Butyrolactone. *The Electrochemical Society* **1994**, *141* (12). DOI: 10.1149/1.2059336.
(74) Peruzzi, N.; Lo Nostro, P.; Ninham, B. W.; Baglioni, P. The Solvation of Anions in Propylene Carbonate. *Journal of Solution Chemistry* **2015**, *44* (6), 1224-1239. DOI: 10.1007/s10953-015-0335-z
(75) Tellinghuisen, J. Isothermal titration calorimetry at very low c. *Analytical Biochemistry* **2008**, *373* (2), 395-397.
(76) Turnbull, W. B.; Daranas, A. H. On the Value of c: Can Low Affinity Systems Be Studies by Isothermal Titration Calorimetry? *Journal of the American Chemical Society* **2003**, *125* (48), 14859-14866.
(77) Haneke, L.; Frerichs, J. E.; Heckmann, A.; Lerner, M. M.; Akbay, T.; Ishihara, T.; Hansen, M. R.; Winter, M.; Placke, T. Editors' Choice—Mechanistic Elucidation of Anion Intercalation into Graphite from Binary-Mixed Highly Concentrated Electrolytes via Complementary ^{19}F MAS NMR and XRD Studies. *Journal of The Electrochemical Society* **2020**, *167* (14), 140526. DOI: 10.1149/1945-7111/abc437
(78) Alia, J. M.; Howell, G. M. E.; Lawson, E. E. Preferential solvation and ionic association in lithium and silver trifluromethanesulfonate solutions in acrylonitrile/dimethylsulfoxide mixed solvent. A Raman spectroscopic study. *Vibrational Spectroscopy* **2003**, *34*, 187-197.
(79) Agostini, M.; Scrosati, B.; Hassoun, J. An Advanced Lithium-Ion Sulfur Battery for High Energy Storage. *Advanced Energy Materials* **2015**, *5* (16), 1500481. DOI: 10.1002/aenm.201500481
(80) Jeong, S.-K.; Inaba, M.; Iriyama, Y.; Abe, T.; Ogumi, Z. Surface film formation on a graphite negative electrode in lithium-ion batteries: AFM study on the effects of co-solvents in ethylene carbonate-based solutions. *Electrochimica Acta* **2002**, *47* (12), 1975-1982.
(81) Morita, M.; Asai, Y.; Yoshimoto, N.; Ishikawa, M. A Raman spectroscopic study of organic electrolyte solutions based on binary solvent systems of ethylene carbonate with low viscosity solvents which dissolve different lithium salts. *Journal of the Chemical Society, Faraday Transactions* **1998**, *94* (23), 3451-3456. DOI: 10.1039/a806278a
(82) Li, T.; Balbuena, P. B. Theoretical Studies of Lithium Perchlorate in Ethylene Carbonate, Propylene Carbonate, and Their Mixtures. *Journal of The Electrochemical Society* **1999**, *146* (10), 3613-3622. DOI: 10.1149/1.1392523

A. Appendix

A1. Thermodynamic Solvent Displacement Model

Binding Polynomial Derivation and Assumptions

Consider a cation as a molecule with N identical binding sites. Each site is occupied by a ligand. In the context of this work, the ligands are solvents S1 and S2. The cumulative displacement of S1 by S2 can be described generally by the chemical equation:

$$\mathrm{M^+(S1)_N + i(S2) \rightleftharpoons M^+(S1)_{N-i}\,(S2)_i + i(S1)} \tag{1}$$

where M^+ is the metal cation, and i=1,2,⋯,N. The relevant equilibrium constant, also known as the stability constant when defined in a cumulative manner, is then:

$$\beta_i = \frac{\{\mathrm{M^+(S1)_{N-i}\,(S2)_i}\}\{\mathrm{S1}\}^i}{\{\mathrm{M^+(S1)_N}\}\{\mathrm{S2}\}^i} \tag{2}$$

where $\{Y\} = e^{\frac{\mu_Y - \mu_Y^\theta}{RT}}$ represents the thermodynamic activity of species Y. The activities can also be written as $\{Y\} = \gamma_Y X_Y$, where γ_Y is the activity coefficient and X_Y is the mole fraction of species Y.

Next, we define a set of 3 mass balance equations, one for each molecule involved in the reaction:

$$X_{M^+,tot} = \sum_{i=0}^{N} X_{M^+(S1)_{N-i}(S2)_i} \tag{3a}$$

$$X_{S1,tot} = X_{S1} + \sum_{i=0}^{N} (N-i) X_{M^+(S1)_{N-i}(S2)_i} \tag{3b}$$

$$X_{S2,tot} = X_{S2} + \sum_{i=0}^{N} i X_{M^+(S1)_{N-i}(S2)_i} \tag{3c}$$

Note that X_{S1} and X_{S2} are the mole fractions of the respective solvents in the uncoordinated state. Using equation (3a) and the relationship $X_Y = \frac{\{Y\}}{\gamma_Y}$, we can define the binding polynomial $Z = \frac{X_{M^+,tot}}{X_{M^+(S1)_N}}$, which is a partition function for the system:

$$X_{M^+,tot} = \sum_{i=0}^{N} \frac{\{M^+(S1)_{N-i}(S2)_i\}}{\gamma_{M^+(S1)_{N-i}(S2)_i}}$$

$$X_{M^+,tot} = \sum_{i=0}^{N} \frac{\{M^+(S1)_N\}}{\gamma_{M^+(S1)_{N-i}(S2)_i}} \beta_i \left(\frac{\{S2\}}{\{S1\}}\right)^i$$

$$Z = \frac{X_{M^+,tot}}{X_{M^+(S1)_N}} = \sum_{i=0}^{N} \frac{\gamma_{M^+(S1)_N}}{\gamma_{M^+(S1)_{N-i}(S2)_i}} \beta_i \left(\frac{\{S2\}}{\{S1\}}\right)^i$$

To continue further, we must make an assumption that the activity coefficient of the cation complex does not change significantly upon solvent displacement such that $\frac{\gamma_{M^+(S1)_N}}{\gamma_{M^+(S1)_{N-i}(S2)_i}} \approx 1$. At very dilute concentrations (< 10^{-3} M), this assumption holds. However, at 0.1M this assumption may be a significant source of error for the model since the displacement of solvent can change the local dielectric constant and alter how the cations interact with nearby solvents and ions. Continuing with this assumption however, the binding polynomial is defined as:

$$Z = \frac{X_{M^+,tot}}{X_{M^+(S1)_N}} = \sum_{i=0}^{N} \beta_i \left(\frac{\{S2\}}{\{S1\}}\right)^i \tag{4}$$

And the mole fraction of any species can be written as:

$$X_{M^+(S1)_{N-i}(S2)_i} = X_{M^+,tot} \frac{\beta_i \left(\frac{\{S2\}}{\{S1\}}\right)^i}{Z} \tag{5}$$

Plugging equation (5) into equations (3b) and (3c) and assuming the solvents follow ideal Rault's Law behavior ($\gamma_{S1} = \gamma_{S2} = 1$)

$$\begin{cases} X_{S1,tot} = X_{S1} + X_{M^+,tot} \sum_{i=0}^{N} \frac{(N-i)\beta_i \left(\frac{X_{S2}}{X_{S1}}\right)^i}{Z} \\ X_{S2,tot} = X_{S2} + X_{M^+,tot} \sum_{i=0}^{N} \frac{i\beta_i \left(\frac{X_{S2}}{X_{S1}}\right)^i}{Z} \end{cases} \tag{6}$$

This leaves two equations and two unknowns: X_{S1} and X_{S2}. Solve (6) and use equation (5) to compute the mole fraction of any cation complex.

Calculating the Expected Electrochemical Cell Potential

The emf of the electrochemical cell of the form:

$$M \left| \begin{matrix} M^+ \ (S1) \\ ref \end{matrix} \right\| \begin{matrix} \text{Salt} \\ \text{Bridge} \end{matrix} \left\| \begin{matrix} M^+ \ (S1+S2) \\ test \end{matrix} \right| M^+$$

Is expected to be related to the difference in free energies of the M^+ solvation environments.

$$E_{cell} = -\frac{\Delta G_{cell}}{zF} = -\frac{1}{zF}\left(G_{M^+,test} - G_{M^+,ref}\right) \tag{7}$$

where z is the charge transferred, and F is the Faraday constant. The free energy of M^+ can represented in terms of its activity.

$$G_{M^+,ref} = G^0_{M^+} + RT\ln(\{M^+\}_{ref}) \tag{8a}$$

$$G_{M^+,test} = G^0_{M^+} + RT\ln(\{M^+\}_{test}) \tag{8b}$$

where $G^0_{M^+}$ is the standard free energy of M^+, and $\{M^+\}$ is the activity of Li^+ in the respective electrolyte. In the context of our binding model, we can write $\{M^+\}$ in terms of the activity of the weak coordination complex by considering the following chemical equilibrium:

$$M^+ + N(S1) \rightleftharpoons M^+(S1)_N$$

From which we can define an association constant:

$$K_A = \frac{\{M^+(S1)_N\}}{\{M^+\}\{S1\}^N} \tag{9}$$

We can then use equation (8a), (8b), and (9) to rewrite equation (7). Note that since K_A is a constant, it will cancel out.

$$E_{cell} = -\frac{\Delta G_{cell}}{zF} = -\frac{RT}{zF}\left(\ln\left(\frac{\{M^+(S1)_N\}_{test}}{\{M^+(S1)_N\}_{ref}}\right) - N\ln\left(\frac{\{S1\}_{test}}{\{S1\}_{ref}}\right)\right) \tag{10}$$

From here, we make a couple assumptions to simplify further. First, we can write $\{M^+(S1)_N\} = \gamma_{M^+(S1)_N} X_{M^+(S1)_N}$. We assume here that $\gamma_{M^+(S1)_N,ref} \approx \gamma_{M^+(S1)_N,test}$, such that $\frac{\{M^+(S1)_N\}_{test}}{\{M^+(S1)_N\}_{ref}} \approx \frac{X_{M^+(S1)_N,test}}{X_{M^+(S1)_N,ref}}$. Furthermore, since there is only one solvent in the reference electrolyte, we can say that $X_{M^+(S1)_N,ref} = X_{M^+,tot,ref}$. Second, we once again assume ideal Rault's law behavior of the solvents. With these assumptions, and the binding polynomial, equation (4), we get to our final equation for the electrochemical cell potential:

$$E_{cell} = -\frac{\Delta G_{cell}}{zF} = -\frac{RT}{zF}\left(\ln\left(\frac{X_{M^+,tot,test}}{X_{M^+,tot,ref}}\right) - \ln(Z_{test}) - N\ln\left(\frac{X_{S1,test}}{X_{S1,ref}}\right)\right) \tag{10}$$

Identical Binding Site Statistical Considerations

If we consider binding sites on a cation to be independent and identical, we can make some simplifications to the above model. Namely, instead of defining a stability constant (β_i) and enthalpy (ΔH_i) for the formation of each possible complex, we can define a single equilibrium constant and enthalpy associated with solvent displacement on any cation binding site, written here as $\mathcal{K}$ and $\Delta\mathcal{H}$,

respectively. These single-site descriptors can be used to calculate the cumulative complex thermochemical parameters β_i and ΔH_i.

Calculating ΔH_i is straightforward. If there are i displacements, and each displacement has an associated enthalpy change of $\Delta\mathcal{H}$, then:

$$\Delta H_i = i\Delta\mathcal{H} \tag{11}$$

Calculating β_i requires consideration of the number of binding sites available for solvent replacement as described by other workers.[48, 60] This can be treated similarly to combinatorial considerations for the free energy of mixing or surface adsorption. Consider a cation with N binding sites, which are all occupied by the weak solvent, S1. There is only $W_0 = \binom{N}{0} = 1$ way the binding sites can be filled. A strong solvent, S2, has N possible sites from which it can displace a weak solvent. The number of possible configurations of binding site occupancies after the first displacement is then $W_1 = \binom{N}{1}$. Similarly, after the i'th displacement, $W_i = \binom{N}{i}$. The change in possible binding site occupancy configurations results in a combinatorial (entropic) change in energy:

$$\Delta S_{comb,i} = k_B \ln\left(\frac{W_i}{W_{i-1}}\right) = k_B \ln\left(\frac{N - i + 1}{i}\right) \tag{12}$$

Equation (12) can be used to relate the stepwise equilibrium constants via the following relationship:

$$K_i = e^{-\frac{\Delta G_i}{k_B T}} = e^{\frac{\Delta G_i'}{k_B T} + \frac{\Delta S_{comb,i}}{k_B}} = \left(\frac{N - i + 1}{i}\right) e^{\frac{\Delta G_i'}{k_B T}} \tag{13}$$

where $\Delta G_i'$ is the stepwise free energy change without the combinatorial contribution. Assuming completely independent and identical binding sites, $\Delta G_i'$ should be constant, and we can write:

$$K_i = \left(\frac{N - i + 1}{i}\right)\mathcal{K} \tag{14}$$

where $\mathcal{K}$ is the single-site equilibrium constant. We can convert this to a stability constant simply:

$$\beta_i = \prod_{j=1}^{i} K_j = \prod_{j=1}^{i} \left(\frac{N - j + 1}{j}\right) \mathcal{K} \tag{15}$$

Note that $\beta_N = \mathcal{K}^N$, and therefore $\mathcal{K}$ can be thought of as the geometric average of the whole solvent displacement equilibrium constant, $\mathcal{K} = (\beta_N)^{1/N}$.

A2. Supplemental Figures & Tables

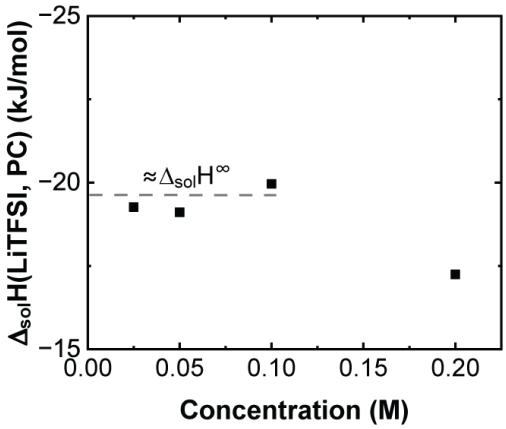

Figure A.1: ***Concentration dependence of $\Delta_{sol}H(LiTFSI, PC)$.*** *Below concentrations of 0.1M LiTFSI, the enthalpy of solution is stable (±1 kJ/mol) and can approximate 'infinite' dilution in PC.*

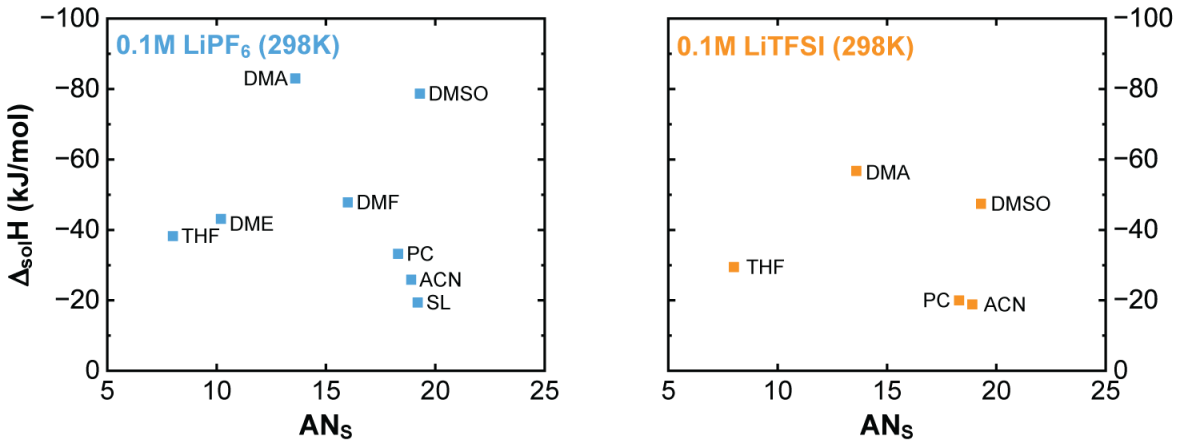

Figure A.2: ***Enthalpies of solution of $LiPF_6$ and LiTFSi in several polar aprotic solvents vs the solvent acceptor number (AN).***

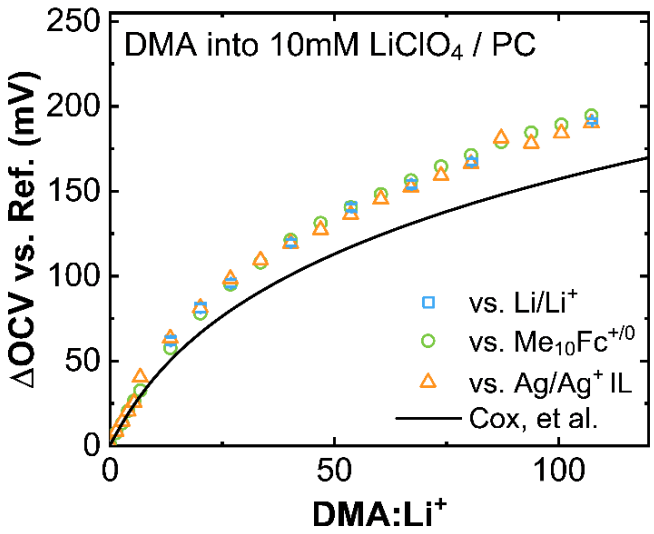

Figure A.4: ***Comparison of reference potentials for potentiometric titrations.*** *The change in OCV of the electrochemical cell during the titration of DMA into a 10mM $LiClO_4$ in PC electrolyte. The Li/Li^+ reference is in a 10mM $LiClO_4$ in PC electrolyte with a 1M LiTFSI DOL:DME salt bridge. Electrolytes separated via glass frits. The $Me_{10}Fc^{+/0}$ redox potential was found via cyclic voltammetry after each injection. The Ag/Ag^+ reference is 10mM AgOtf in $[N_{2225}]^+[TFSI]^-$ ionic liquid, separated with a glass frit. The solid line is the expected ΔOCV reconstructed from binding constants reported in Cox, et al.* J. Chem. Soc., Faraday Trans. 1 ***1976***.[2]

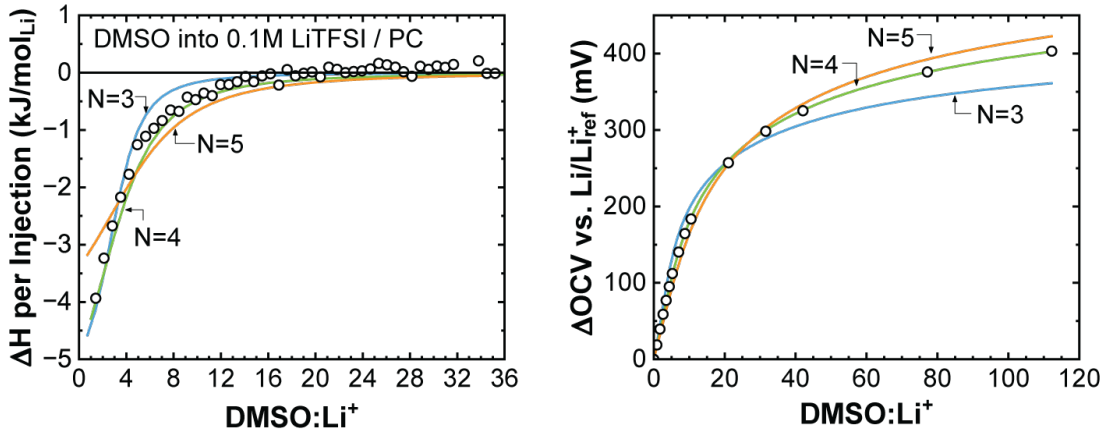

Figure A.3: ***Comparison of the number of binding sites, N, used in the binding model.*** *The experimental data from the calorimetric (left) and potentiometric (right) titrations of DMSO into 0.1M LiTFSI in PC are shown as open circles. Solid lines are best fits from binding models with N=3,4,5 binding sites.*

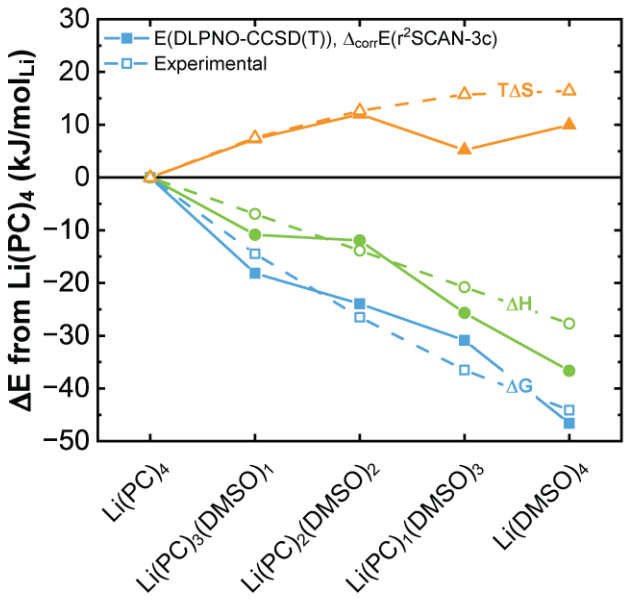

Figure A.5: ***Comparison of DFT computed and experimental relative Li$^+$-PC-DMSO complex thermodynamics.*** *Complex geometries were optimized and frequency calculations were conducted using the r^{2}SCAN-3c composite method. Complex electronic energies were calculated at the more accurate DLPNO-CCSD(T)/def2-TZVPD level.*

Table A.1: ***Enthalpies of injection of DMSO into a PC electrolyte with 0.1M salt concentration.*** *The end state after an injection is a 0.08M PC:DMSO (4:1 vol) electrolyte.*

Salt	$\boldsymbol{\Delta_{inj}H\left(salt,\ 0.1M\ PC \rightarrow \begin{matrix}0.08M\ PC:DMSO\\(4:1\ vol)\end{matrix}\right)}$
$LiClO_4$	-29.23 ± 1.0
$LiPF_6$	-24.83 ± 4.6
LiTFSI	-27.89 ± 0.7
LiFSI	-29.96 ± 2.3
$TBAClO_4$	-0.62 ± 0.2
$TBAPF_6$	-0.25 ± 0.2
TBATFSI	-0.49 ± 0.2
Ph_4PI	-2.87 ± 0.3
$NaPh_4B$	-17.37 ± 0.1
NaI	-24.34 ± 0.3
NaTFSI	-17.80 ± 0.2

*Table A.2****: Single ion enthalpies of injection of DMSO into a PC electrolyte with 0.1M ion concentration.*** *The end state after an injection is a 0.08M PC:DMSO (4:1 vol) electrolyte. The TPTP assumption was used to obtain the single ion contributions.*

Ion	$\boldsymbol{\Delta_{inj}H\left(I^{\pm},\ 0.1M\ PC \rightarrow \begin{matrix}0.08M\ PC:DMSO\\(4:1\ vol)\end{matrix}\right)}$
Cations	
Li^+	-28.98 ± 3.1
Na^+	-19.42 ± 0.5
TBA^+	-2.11 ± 0.9
Ph_4P^+	2.05 ± 0.4
Anions	
PF_6^-	1.86 ± 1.1
$TFSI^-$	1.62 ± 0.7
ClO_4^-	1.49 ± 1.2
FSI^-	-0.98 ± 5.4
I^-	-4.92 ± 0.6
Ph_4B^-	2.05 ± 0.4